

NASA TECHNICAL NOTE



NASA TN D-7651

NASA TN D-7651



CAP...
CHAR...
SHARP...
45...

...
...
... (M...)

...
... 4008

**THEORETICAL AND EXPERIMENTAL
LONGITUDINAL AERODYNAMIC CHARACTERISTICS
OF AN ASPECT RATIO 0.25 SHARP-EDGE
DELTA WING AT SUBSONIC, SUPERSONIC,
AND HYPERSONIC SPEEDS**

by Charles H. Fox, Jr., and John E. Lamar

Langley Research Center

Hampton, Va. 23665



1 Report No. NASA TN D-7651	2 Government Accession No.	3 Recipient's Catalog No.	
4 Title and Subtitle THEORETICAL AND EXPERIMENTAL LONGITUDINAL AERO-DYNAMIC CHARACTERISTICS OF AN ASPECT RATIO 0.25 SHARP-EDGE DELTA WING AT SUBSONIC, SUPERSONIC, AND HYPERSONIC SPEEDS		5 Report Date August 1974	
		6 Performing Organization Code	
7 Author(s) Charles H. Fox, Jr., and John E. Lamar		8 Performing Organization Report No. L-9328	
		10 Work Unit No. 501-06-04-01	
9 Performing Organization Name and Address NASA Langley Research Center Hampton, Va. 23665		11 Contract or Grant No.	
		13 Type of Report and Period Covered Technical Note	
12 Sponsoring Agency Name and Address National Aeronautics and Space Administration Washington, D.C. 20546		1 Sponsoring Agency Code	
		15 Supplementary Notes Appendix A, entitled "Influence of Ground Proximity on Longitudinal Aerodynamic Characteristics of an Aspect Ratio 0.25 Delta Wing," is by Charles H. Fox, Jr., John E. Lamar, and W. Pelham Phillips.	
16 Abstract <p>The suction analogy concept of Polhamus for predicting vortex lift in conjunction with an appropriate potential-flow solution is called the present method. This method is applied herein to an aspect ratio 0.25 sharp-edge delta wing from a Mach number of 0.143 to 10.4 in free air and at 0.074 in ground effect, and also to an aspect ratio 0.35 triangular cross-sectional body at a Mach number of 6.9. The models had subsonic leading edges at the test Mach numbers. Vortex-flow effects could be neither confirmed nor denied to exist at high speeds because of the lack of flow visualization above a Mach number of 0.143. The data, however, could be better predicted by including a vortex-flow effect, although not always to the extent predicted from the present method because of the presence of actual and hypothesized unmodeled flow situations. The method of Nenni and Tung (NASA CR-1860) tended to confirm the existence of vortex flow at hypersonic speeds. The hypersonic-tangent-cone method predicted best the delta-wing results over the test angle-of-attack range and hypersonic Mach number range and did equally as well as the present method for the triangular body.</p>			
17. Key Words (Suggested by Author(s)) Low-aspect-ratio delta wing Sharp edge Theory Experiment		Subsonic Supersonic Hypersonic	18. Distribution Statement Unclassified - Unlimited STAR Category 01
19. Security Classif. (of this report) Unclassified	20. Security Classif. (of this page) Unclassified	21. No. of Pages 43	22. Price* \$3.25

THEORETICAL AND EXPERIMENTAL LONGITUDINAL AERODYNAMIC
CHARACTERISTICS OF AN ASPECT RATIO 0.25 SHARP-EDGE
DELTA WING AT SUBSONIC, SUPERSONIC, AND
HYPERSONIC SPEEDS

By Charles H. Fox, Jr., and John E. Lamar
Langley Research Center

SUMMARY

The suction analogy concept of Polhamus for predicting vortex lift in conjunction with an appropriate potential-flow solution is called the present method. This method is applied herein to an aspect ratio 0.25 sharp-edge delta wing from a Mach number of 0.143 to a Mach number of 10.4 in free air and at a Mach number of 0.074 in ground effect, and also to an aspect ratio 0.35 triangular cross-sectional body at a Mach number of 6.9. The models had subsonic leading edges at the test Mach numbers. Vortex-flow effects could be neither confirmed nor denied to exist at high speeds because of the lack of flow visualization above a Mach number of 0.143. The data, however, could be better predicted by including a vortex-flow effect, although not always to the extent predicted from the present method because of the presence of actual and hypothesized unmodeled flow situations. The method of Nenni and Tung (NASA CR-1860) tended to confirm the existence of vortex flow at hypersonic speeds. The hypersonic-tangent-cone method predicted best the delta-wing results over the test angle-of-attack range and hypersonic Mach number range and did equally as well as the present method for the triangular body.

INTRODUCTION

The leading-edge suction analogy of Polhamus (ref. 1) in conjunction with a potential-flow solution appropriate to the given Mach number has been used successfully to predict the nonlinear aerodynamic characteristics of sharp-edge delta wings over a wide range of aspect ratios (refs. 1 and 2) at both subsonic and supersonic speeds (ref. 3). This procedure, referred to hereafter as the present method, is applicable so long as the symmetrical leading-edge shed vortices and flow reattachment are present, thereby necessitating a subsonic flow in the vicinity of the leading edge. For highly swept delta wings, the flow normal to the leading edges should be subsonic even with the wing traveling at hypersonic speeds. Therefore, wind-tunnel tests at hypersonic, supersonic, and subsonic speeds were conducted for such a wing (0.25 in aspect ratio) to investigate

whether vortex-flow effects could be discerned from the static longitudinal data by using the present method. Other theoretical predictions are also made for comparisons in the various speed regimes.

Two appendixes to the present paper are included. Appendix A presents basic ground-effect data for this wing at a low subsonic Mach number. These data can serve as a lower aspect-ratio limit in delta-wing ground-effect studies. Limited comparisons between these data and the present method are made. Appendix B repeats some basic data on a triangular cross-sectional body having a subsonic leading edge at a moderate hypersonic speed (ref. 4) and compares the data with the present and hypersonic methods.

SYMBOLS

The force and moment data are referred to the stability-axis system for the longitudinal characteristics. Values are given in both SI and U.S. Customary Units. The measurements and calculations were made in U.S. Customary Units.

b	wing span, m (ft)
C_D	drag coefficient, Drag/qS
C_{D_0}	drag coefficient at zero lift
$C_{D_{min}}$	minimum drag coefficient
C_L	lift coefficient, Lift/qS
C_l	rolling-moment coefficient, Rolling moment/qSb
C_m	pitching-moment coefficient about half root chord (which for delta wing is also quarter chord of wing mean geometric chord), Pitching moment/qS \bar{c}
C_N	normal-force coefficient, Normal force/qS
C_S	leading-edge-suction coefficient, 2(Single-edge suction force)/qS
\bar{c}	wing mean geometric chord, m (ft)

c_r	root chord, m (ft)
$h_{\bar{c}/4}$	height above ground of location of quarter chord of wing mean geometric chord, m (ft)
K_p	potential-flow normal-force parameter, $\partial C_N / \partial (\sin \alpha \cos \alpha)$
K_v	potential-flow leading-edge suction-force parameter, $\partial C_S / \partial (\sin^2 \alpha)$
L/D	lift-drag ratio
M	free-stream Mach number
q	free-stream dynamic pressure, N/m ² (lbf/ft ²)
R	Reynolds number based on wing root chord
S	wing reference area, m ² (ft ²)
x	coordinate with origin at apex nondimensionalized with respect to wing root chord, positive aft
α	angle of attack, deg
α_d	angle of attack at which lift curves for experiment and present method depart, deg

Subscripts:

c	centroid of normal force
p	attached or potential-flow theory
ref	moment reference point
v	vortex-lift increment based on leading-edge suction analogy

MODELS

Three geometrically similar models of an aspect ratio 0.25 sharp leading-edge delta wing were used in the experimental study because of the various size restraints imposed by the different speed wind tunnels. The geometrical characteristics of the models are presented in table I and figure 1. The figure shows that the models are composed of the basic wing planform, a balance housing, and either a partial-chord sharp-edge ventral fin or a full-chord blunt-edge dorsal fin used to stiffen the wing apex region.

Photographs of three model installations are presented in figure 2. Figure 2(a) shows the lower surface of the subsonic model prior to testing. Initial tests with this model indicated a yaw instability, due to the fin not extending the full length of the root chord, which was subsequently corrected by employing a substantial vertical tail, as shown in figure 1(a).

The fin and vertical tail of the subsonic model were tested in the ventral position so as not to interfere with the leading-edge shed vortices.

TESTS, MEASUREMENTS, AND CORRECTIONS

Because the data of the present investigation were obtained in a number of facilities (described in ref. 5), the following table has been prepared to give the pertinent test conditions:

Facility	M	$R \times 10^{-6}$
Langley 300-MPH 7- by 10-foot tunnel, 17-foot test section	0.074	3.6
Langley high-speed 7- by 10-foot tunnel	.143	6
Langley Unitary Plan wind tunnel, test section 2	2.30 to 4.63	9
Langley 20-inch hypersonic tunnel (Mach 6)	5.99	7.5
Langley continuous-flow hypersonic tunnel	10.40	11.7

Aerodynamic forces and moments were measured by means of a six-component electrical strain-gage balance housed within the model. The measured data have been corrected for balance deflections under load, and the drag data are adjusted to a condition corresponding to free-stream static pressure in the balance cavity.

The subsonic and hypersonic tests were run transition free. However, the supersonic tests at $M = 2.30$ to 4.63 were made with transition strips of individual grains of No. 40 sand near the leading edge of both the upper and lower surfaces. These sand grains are clearly visible in figure 2(b).

THEORETICAL METHODS

Three theoretical methods are compared with the experimental data. They are referred to as: (1) Attached (potential) flow, (2) present, and (3) hypersonic tangent cone. The attached-flow method and the present method (which assumes a leading-edge vortex type of flow) are applied in all three experimental speed regimes to predict the static longitudinal aerodynamic characteristics. The hypersonic-tangent-cone method is applied only above Mach 1.

The equations for the lift and drag characteristics for the attached-flow method and for the present method are found in reference 2 and are

$$C_L = C_{L,p} + C_{L,v} = C_{N,p} \cos \alpha + C_{N,v} \sin \alpha \quad (1)$$

or

$$C_L = K_p \sin \alpha \cos^2 \alpha + K_v \sin^2 \alpha \cos \alpha \quad (2)$$

and

$$C_D = C_L \tan \alpha + C_{D_0} \quad (3)$$

where for the potential-flow method $K_v = 0$ and zero leading-edge suction is assumed.

The pitching-moment-coefficient equation is given in reference 6 as

$$C_m = \frac{c_r}{\bar{c}} \left[(x_{ref} - x_{c,p}) C_{N,p} + (x_{ref} - x_{c,v}) C_{N,v} \right] \quad (4)$$

The dependence of K_p and K_v on Mach number as determined from references 1 to 3 is summarized for this wing in figure 3. Note from the figure that K_v does not become zero (thereby indicating a supersonic leading edge) until a hypersonic

Mach number much higher than the highest test speed is reached; therefore, leading-edge separation and vortex lift would be expected over the complete range of Mach numbers of this investigation.

From equation (4), the pitching-moment computation is seen to require the locations of the potential and vortex normal-force centroids at subsonic, supersonic, and hypersonic speeds. The following discussion assumes that the longitudinal location of the centroid of the vortex normal-force distribution is the same as the longitudinal location of the centroid of the leading-edge suction distribution and thereby ignores any longitudinal shift that may occur as the vortex moves inboard from the leading edge.

At subsonic speeds the potential and vortex normal-force centroids are determined from the distribution of the attached-flow loading and the leading-edge suction, respectively, as computed by the method of reference 7. These centroids are Mach number dependent, and for $M = 0.143$ are determined to be $0.65456c_r$ and $0.66664c_r$, respectively, thereby reducing the equation for pitching moment at $M = 0.143$ to

$$C_m = -0.23188 \frac{C_{L,p}}{\cos \alpha} - 0.24996 \frac{C_{L,v}}{\cos \alpha} \quad (5)$$

At both supersonic and hypersonic speeds, the supersonic potential normal-force centroid is found to be $\frac{2}{3}c_r$ based on the conical-flow assumption of reference 8. The distribution of leading-edge suction along the leading edge of a delta wing at supersonic speeds can also be determined on the basis of conical flow. The centroid of this distribution is also found to be $\frac{2}{3}c_r$ as determined from reference 9. Substituting these values in equation (4) results in

$$C_m = -\frac{1}{4} \frac{C_L}{\cos \alpha} \quad (6)$$

for supersonic and hypersonic speeds. The assumption of conical flow leads to a linear distribution for both the attached flow and the leading-edge suction loading and causes the predicted static margin to be independent of Mach number at supersonic and hypersonic speeds in contrast to the variation with Mach number at subsonic speeds.

The aerodynamic predictions with the potential-flow method are easily made in all three speed regimes once K_p is known. The equations employed (eqs. (1) to (4)) are the same as for the present method with $K_v = 0$.

At supersonic and hypersonic speeds the hypersonic-tangent-cone method has also been used. This method employs a tangent-cone solution on the windward side of the model and a Prandtl-Meyer expansion solution on the leeward side (ref. 10). The author of reference 11 determined this method to be satisfactory in predicting the hypersonic aerodynamic characteristics of a highly swept sharp leading-edge wing-body combination;

hence, it was adopted for use herein. James C. Ellison of NASA Langley Research Center obtained the hypersonic-tangent-cone results presented herein by employing the computer program of reference 10.

RESULTS AND DISCUSSION

The basic static longitudinal experimental data along with the theoretical predictions are presented in figure 4 for Mach numbers of 0.143, 2.30, 2.96, 3.95, 4.63, 5.99, and 10.40. The comparisons between the data and the theoretical predictions are discussed separately for each analytical method.

Attached- (Potential-) Flow Method

As expected the potential-flow results depart rapidly from the experimental lift and drag data as the angle of attack is increased. For α greater than zero, the sharp leading edges produce a separation and detached flow which is not modeled by this method. Good agreement was found with the pitching-moment data at all lift coefficients for Mach numbers less than 6 because of the closeness of the longitudinal load centroid of the potential-flow method and the experimental results.

Present Method

Because the present method contains the potential-flow method as one term in its equations for C_L and C_m , then at low angles of attack the two methods yield essentially the same results. As α or C_L increases, the present method gives much better agreement than attached flow with the experimental lift and drag values because of the inclusion of the influence of flow detachment. This agreement continues up to moderate angles of attack, but the range of agreement decreases with increasing Mach number. This result is shown in figure 5 which presents the angle-of-attack range in which the values of C_L for the present method and experiment begin to depart at the various test Mach numbers. Figure 6 shows that, at the lowest Mach number, the model suddenly experiences a large rolling moment indicative of vortex asymmetry occurring near the angle of attack cited for departure. Similar rolling-moment behavior was noted on high-fineness-ratio bodies in reference 12. Smoke studies confirmed the presence of asymmetric vortexes at low subsonic speeds and at the angle of attack cited for departure for both the free-air test and the test in ground effect. (See also appendix A.) However, at the higher Mach numbers the rolling-moment data indicated no such asymmetry; hence, the reason for the earlier departure of the theoretical (present method) and experimental lift curves with increasing Mach number must be attributable to some flow phenomena

other than vortex asymmetry. Because the wing is so slender, the breakdown of the vortex ahead of the trailing edge is not anticipated (ref. 3).

Reference 3 shows that, as the supersonic Mach number increases, the value of K_v (see fig. 3) and the associated vortex size become smaller. These reductions are due to the approach of the shock cone to the wing leading edge and the subsequent reduction in the extent and strength of the upwash field. These relationships can be more clearly understood if it is recognized that the amount of flow entrained in a leading-edge vortex is dependent on the extent and strength of the upwash field. The vortex lift is attributed physically to this flow entrainment and is approximated well mathematically by

$$\text{Vortex lift} = qSK_v \sin^2 \alpha \cos \alpha \quad (7)$$

Hence, any limiting of the upwash field will reduce the amount of flow entrainment and subsequently require a smaller value of K_v . Note further that a fixed vortex lift can be obtained by a combination of the extent and strength of the upwash field or, correspondingly, by a combination of Mach number and angle of attack in equation (7).

A basic assumption in the present method is that, as the angle of attack increases, the leading-edge vortex becomes larger and entrains more flow, thereby resulting in an increase in the amount of vortex lift. These increases may not always occur for Mach numbers above 1 because, unlike the subsonic flow which has the wing upwash field transmitted upstream a very large distance, the supersonic upstream transmissions are limited not only within the shock cone, which has been accounted for, but also by the proximity of the wing surface to the cone. Consequently, as the angle of attack increases at a specified Mach number, the wing approaches the lower portion of the shock cone and the extent of the upwash field is correspondingly reduced. This phenomenon was not anticipated in the present method and becomes a problem here in the estimation of vortex lift above $M = 2.30$ and above $\alpha = 5^\circ$, according to figure 5. These considerations have the effect of making K_v a function of angle of attack in equation (7) for Mach numbers above 1. The possibility therefore exists that the suction-analogy concept for predicting K_v may still be valid at the higher angles of attack and the problem is instead with the supersonic theory used for predicting the leading-edge suction because it does not account for the increased proximity that occurs as the wing moves off of the shock-cone axis at increasing angles of attack.

In order to make some rough estimates of the dependency of K_v on α , the model was represented at selected angles of attack by symmetrical cones the semivertex angles of which were the same as the wing angle of attack. By employing the shock tables (ref. 13) to find the Mach number associated with the angular distance between these conical bodies and the associated shock cones, a new K_v was determined from figure 3

based on this equivalent Mach number. This procedure was exercised at several angles of attack at $M = 5.99$ and the resulting vortex-lift values were compared with the original estimations and with the experimental vortex lift (defined for this comparison as that experimental lift in excess of the estimated potential lift). The results are that, whereas the original estimates exceeded the experimental amount by a generally increasing large percentage as the angle of attack increased, the estimates according to the previous approximate procedure were much closer in actual value and, in general, increasingly underestimated the data but by a much smaller percentage. Although this approach must be considered as very approximate, it serves to illustrate the importance of accounting for the effect of angle of attack on the relative position of the wing and the shock cone in computing the leading-edge suction. A more accurate potential-flow representation would be expected to yield better agreement.

The preceding discussion cannot by itself prove or disprove the existence of vortex lift on the models tested, but it does indicate one possible reason for the overprediction of the present method at supersonic and hypersonic speeds. The only ways to prove the existence of vortex flows at the higher speeds are with flow visualization or pressure measurements.

The pitching-moment variation with lift is well predicted over the Mach number range below 6, thereby indicating that, as with the potential-flow method previously discussed, the longitudinal load centroid of the model and this method are very close.

Hypersonic-Tangent-Cone Method

In the range of Mach numbers usually associated with hypersonic speeds (M greater than 3), the hypersonic-tangent-cone method provides the best agreement with the experimental data. Reasonable agreement was anticipated because this method had been determined by the author of reference 11 to predict the data well on sharp leading-edge wing-like configurations up to $M = 6$, which was the reason it was selected for use in the present paper. Even though the hypersonic-tangent-cone method does not model the flow field between the shock cone and the wing and only approximates the pressures, it is sufficiently accurate to estimate the static longitudinal aerodynamic characteristics of the present model above a Mach number of 3.

Additional Comparisons

Figure 7 presents the lift variation with Mach number at two different angles of attack for the present experiment and for several theoretical methods, including the three just discussed. The (a) part of figure 7 summarizes the lift discussion and shows that, in general, the agreement is about the same with either the present method or the

hypersonic-tangent-cone method at $\alpha = 5^\circ$, but that at $\alpha = 10^\circ$, the hypersonic-tangent-cone method does predict better.

Figure 7(b) contains theoretical predictions from three additional methods: (1) Brown and Michael (ref. 14), (2) Mangler and Smith (ref. 15), and (3) Nenni and Tung (ref. 16). The methods of references 14 and 15 use concentrations of vorticity for the shed vortex core but different concepts to model the connection of the vortex core to the wing leading edge. Both are well documented and widely employed in the literature. The method of reference 16 is based on the Brown and Michael crossflow model in conjunction with a second-order correction theory. Joseph P. Nenni of Calspan, Inc., provided the results based on this method. Of these methods, figure 7(b) shows that only results obtained by employing the last method have any variation of lift with Mach number. These results are in reasonable agreement with the experiment over a Mach number range up to $M = 6.5$ and $M = 4.5$ for the low and high angles of attack, respectively.

A comparison of the lift predictions of the hypersonic-tangent-cone method (fig. 7(a)) and the method of reference 16 (fig. 7(b)) at both angles of attack shows excellent agreement between them over the Mach number range which they have in common. The good agreement between the method of reference 16 and the experimental lift tends to confirm the occurrence of vortex flow at angles of attack above which the present method overpredicts the data, thereby indicating the importance of proper vortex-flow modeling.

It is of interest to compare the present and the hypersonic-tangent-cone methods with experimental data for a thick configuration to determine whether the regions of agreement found for the thin wing are the same. Such a comparison is presented in appendix B.

CONCLUSIONS

A sharp-edge delta wing of aspect ratio 0.25 has been tested in wind tunnels at Mach numbers from 0.143 to 10.40. The leading edge was subsonic throughout the Mach number range. The resulting static longitudinal aerodynamic data were compared with theoretical predictions and the following conclusions were drawn:

1. Leading-edge vortex effects could neither be confirmed nor denied to exist, since no flow visualizations were obtained above a Mach number of 0.143; however, the data obtained could be better predicted by taking into account a vortex contribution than without it.

2. The experimental lift was predicted well by the present method (composed of the potential-flow lift plus the vortex lift as originally proposed by Polhamus) until some flow phenomena occurred which caused the vortex to depart from the assumed classical

shape. At the lowest Mach number, vortex asymmetry occurred at an angle of attack of approximately 13° . At higher Mach numbers, flow situations not accurately represented by the assumed model are hypothesized to occur at lower angles of attack.

3. The prediction of lift variation with Mach number made by the method of Nenni and Tung (NASA CR-1860), which accounts for the leading-edge vortex, tended to confirm the existence of vortex lift at angles of attack of 5° and 10° . This method predicted the lift as well as the hypersonic-tangent-cone method (which does not account for the leading-edge vortex), at these angles of attack up to a Mach number of approximately 4.8.

4. The centroid of the model loading is very close to the model centroid of area at all Mach numbers and is well predicted by all theories used in the pitching-moment comparison.

5. The hypersonic-tangent-cone method (tangent cone on the windward side and Prandtl-Meyer expansion on the leeward side) provides the best prediction of the lift, drag, and pitching-moment characteristics for the range of data at Mach numbers above 3.

6. Additional wind-tunnel tests with this model in ground effects at a Mach number of 0.074 show that the present method predicted the lift and drag trends and levels reasonably well below the occurrence of vortex asymmetry.

The comparisons of several theories with the experimental static longitudinal data for an aspect ratio 0.35 triangular cross-sectional body, which at a Mach number of 6.9 had a subsonic leading edge, showed that:

7. The lift, drag, and pitching moment were well predicted by the present method.

8. For this body at a Mach number of 6.9 either the present method or the hypersonic-tangent-cone method would yield equally good results.

Langley Research Center,
National Aeronautics and Space Administration,
Hampton, Va., May 15, 1974.

APPENDIX A

INFLUENCE OF GROUND PROXIMITY ON LONGITUDINAL AERODYNAMIC CHARACTERISTICS OF AN ASPECT RATIO 0.25 DELTA WING

By Charles H. Fox, Jr., John E. Lamar, and W. Pelham Phillips
Langley Research Center

The basic longitudinal data in ground proximity at a Mach number of 0.074 is presented in figure 8 and summarized in figure 9. Note that, following the format of reference 17, figure 9 presents the drag due to lift $C_D - C_{D_{min}}$. The summary data show the expected trends of increasing lift and drag with decreasing height above the ground. The present method gives the same general trends as the data and predicts the values reasonably well until vortex asymmetry occurs at an angle of attack of approximately 13° . Potential-flow results are seen to underpredict all of the data.

At the moderate ground heights, as well as at the higher angles of attack, the lift increment due to ground proximity is lower than might be expected from a comparison with reference 17. However, reference 17 dealt with higher aspect ratios, covering the range from 1.072 to 3.356. The data from reference 17 at $\alpha = 10^\circ$ close to the ground are repeated herein as figure 10 with the results of the present investigation added. This figure shows that the trend of improved prediction capability with decreasing aspect ratio attributed to the present method in reference 17 extends to the low aspect ratio of the present study.

Theoretical pitching-moment results are not presented in ground proximity because the method of reference 17 does not compute the leading-edge suction distribution (only its total value), and hence the location of the suction centroid is not known.

APPENDIX B

LONGITUDINAL AERODYNAMIC CHARACTERISTICS OF AN ASPECT RATIO 0.35 TRIANGULAR BODY AT $M = 6.9$

Basic longitudinal experimental data along with theoretical predictions are presented in reference 4 for a family of triangular cross-sectional bodies. One set of these data is reproduced here (fig. 11) because it is for a model that has a subsonic leading edge when the free-stream Mach number is 6.9. These data provide an opportunity to apply the theoretical methods of the present investigation to a thick nonsymmetrical configuration. The procedure for employing the present method to this model was that of: (a) rotating the suction force normal to the body lateral surface, and (b) taking the component of force acting in the lift direction as the vortex lift.

Along with the experimental data, four theoretical curves are also presented for comparison in figure 11. Three of the curves are determined from theories previously discussed in the present paper, whereas the fourth curve is from reference 4 and is based on hypersonic-shock-expansion theory. The theoretical lift curves for the present and supersonic potential methods were translated (in angle of attack) to pass through the experimental angle for zero lift to compensate for the difference in the definition of angle of attack.

A comparison of the experiment and theories shows that, of the four, only the present method and the hypersonic-tangent-cone method predict results in good agreement with the experiment. The agreement between the present method and the data at the higher angles of attack is different than with the thin-wing results. The reasons for the difference in agreement are not clear, but it is interesting to note that these hypersonic results can be accurately predicted by using the concept that leading-edge vortex flow is present and is contributing to the lift.

REFERENCES

1. Polhamus, Edward C.: A Concept of the Vortex Lift of Sharp-Edge Delta Wings Based on a Leading-Edge Suction Analogy. NASA TN D-3767, 1966.
2. Polhamus, Edward C.: Charts for Predicting the Subsonic Vortex-Lift Characteristics of Arrow, Delta, and Diamond Wings. NASA TN D-6243, 1971.
3. Polhamus, Edward C.: Predictions of Vortex-Lift Characteristics by a Leading-Edge Suction Analogy. J. Aircraft, vol. 8, no. 4, Apr. 1971, pp. 193-199.
4. Peniand, Jim A.: Maximum Lift-Drag-Ratio Characteristics of Rectangular and Delta Wings at Mach 6.9. NASA TN D-2925, 1965.
5. Schaefer, William T., Jr.: Characteristics of Major Active Wind Tunnels at the Langley Research Center. NASA TM X-1130, 1965.
6. Davenport, Edwin E.; and Huffman, Jarrett K.: Experimental and Analytical Investigation of Subsonic Longitudinal and Lateral Aerodynamic Characteristics of Slender Sharp-Edge 74° Swept Wings. NASA TN D-6344, 1971.
7. Wagner, Siegfried: On the Singularity Method of Subsonic Lifting-Surface Theory. AIAA Paper No. 69-37, Jan. 1969.
8. Puckett, A. E.; and Stewart, H. J.: Aerodynamic Performance of Delta Wings at Supersonic Speeds. J. Aeronaut. Sci., vol. 14, no. 10, Oct. 1947, pp. 567-578.
9. Brown, Clinton E.: Theoretical Lift and Drag of Thin Triangular Wings at Supersonic Speeds. NACA Rep. 839, 1946.
10. Gentry, Arvel E.; and Smyth, Douglas N.: Hypersonic Arbitrary-Body Aerodynamic Computer Program (Mark III Version). Vol. II - Program Formulation and Listings. Rep. DAC 61552, Vol. II (Air Force Contract Nos. F33615 67 C 1008 and F33615 67 C 1602), McDonnell Douglas Corp., Apr. 1968. (Available from DDC as AD 851 812.)
11. Ellison, James C.: Investigation of the Aerodynamic Characteristics of a Hypersonic Transport Model at Mach Numbers to 6. NASA TN D-6191, 1971.
12. Spencer, Bernard, Jr.; and Phillips, W. Pelham: Effects of Cross-Section Shape on the Low-Speed Aerodynamic Characteristics of a Low-Wave-Drag Hypersonic Body. NASA TN D-1963, 1963.
13. Ames Research Staff: Equations, Tables, and Charts for Compressible Flow. NACA Rep. 1135, 1953. (Supersedes NACA TN 1428.)
14. Brown, Clinton E.; and Michael, William H., Jr.: On Slender Delta Wings With Leading-Edge Separation. NACA TN 3430, 1955.

15. Mangler, K. W.: and Smith, J. H. B.: Calculation of the Flow Past Slender Delta Wings With Leading Edge Separation. Rep. No. Aero. 2593, Brit. R.A.E., May 1957.
16. Nenni, Joseph P.; and Tung, Chee: A Second Order Slender Wing Theory for Wings With Leading Edge Separation in Supersonic Flow. NASA CR-1860, 1971.
17. Fox, Charles H., Jr.: Prediction of Lift and Drag for Slender Sharp-Edge Delta Wings in Ground Proximity. NASA TN D-4891, 1969.

TABLE I.- GEOMETRIC CHARACTERISTICS OF ASPECT RATIO 0.25 WINGS

Subsonic tests:

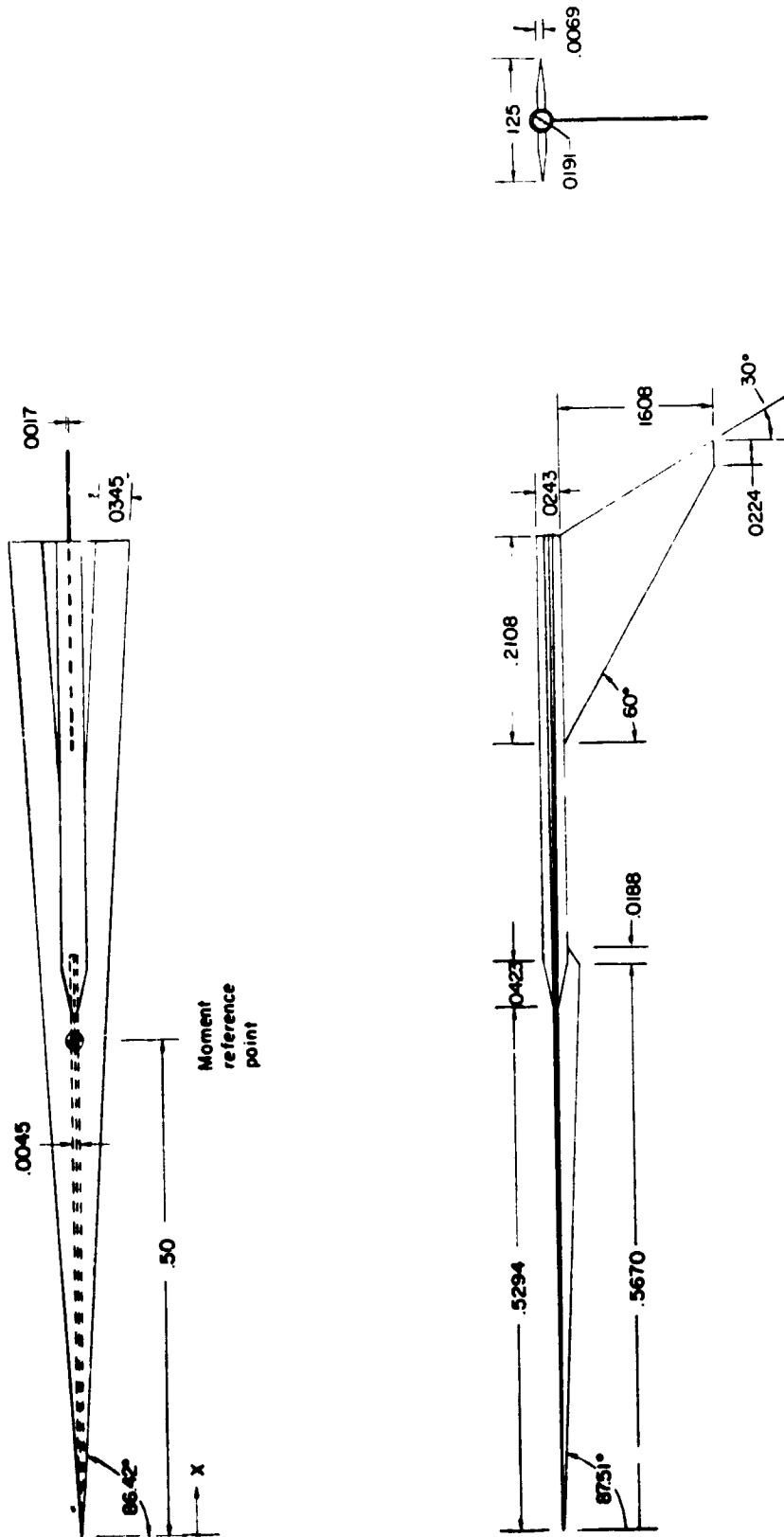
c_r	182.88 cm (72.00 in.)
b	22.86 cm (9.00 in.)
\bar{c}	121.92 cm (48.00 in.)
S	0.2029 m ² (2.25 ft ²)

Supersonic tests:

c_r	91.44 cm (36.00 in.)
b	11.43 cm (4.5 in.)
\bar{c}	60.96 cm (24.00 in.)
S	0.0523 m ² (0.5625 ft ²)

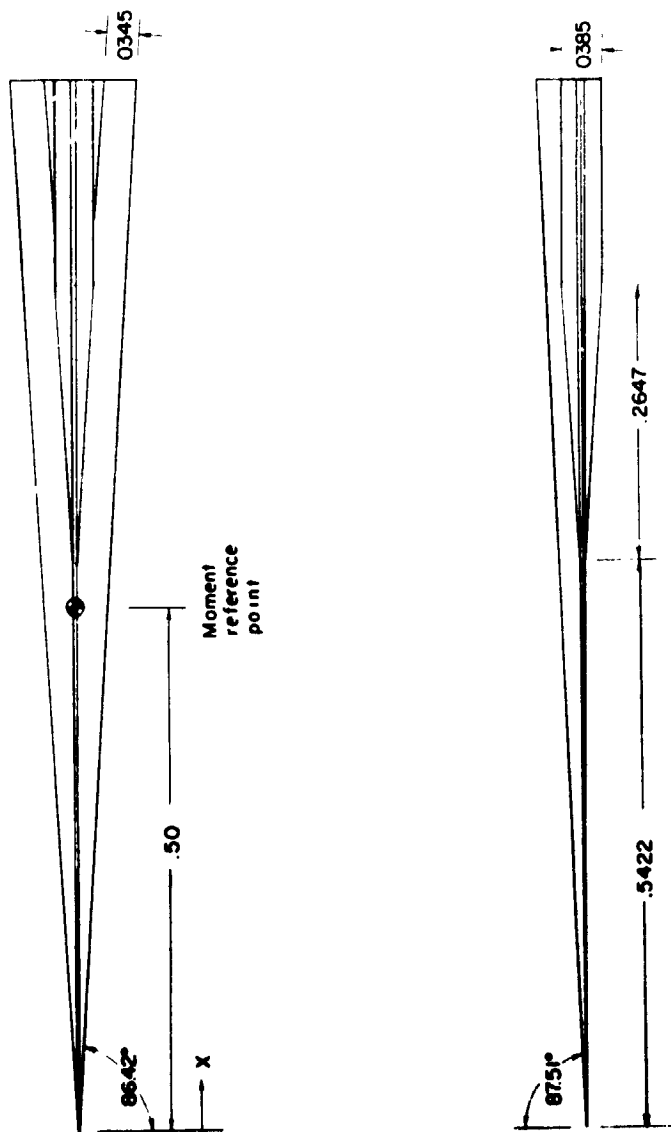
Hypersonic tests:

c_r	76.20 cm (30.00 in.)
b	9.525 cm (3.75 in.)
\bar{c}	50.80 cm (20.00 in.)
S	0.0363 m ² (0.390625 ft ²)



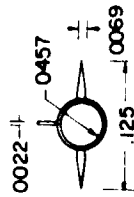
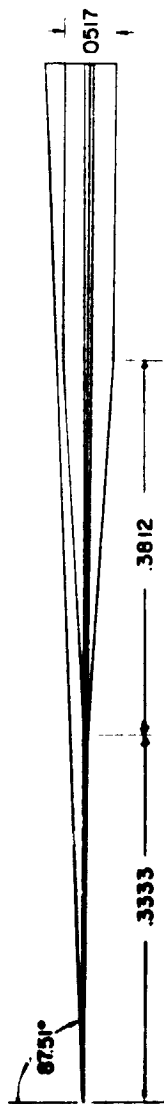
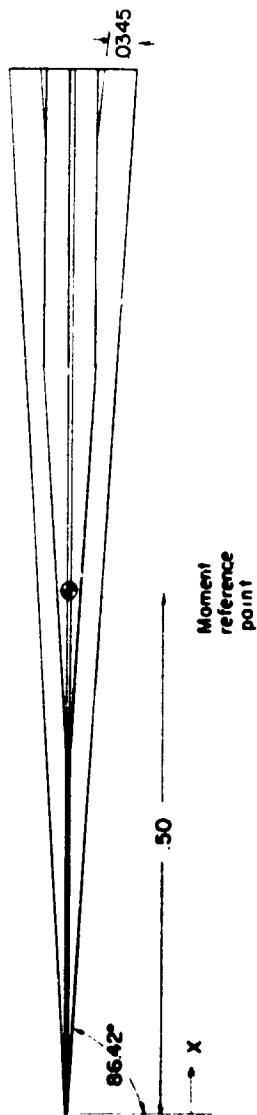
(a) Subsonic model.

Figure 1.- Drawings of models tested. (All dimensions are in fractions of wing root chord.)



(b) Supersonic model.

Figure 1.- Continued.



(c) Hypersonic model.

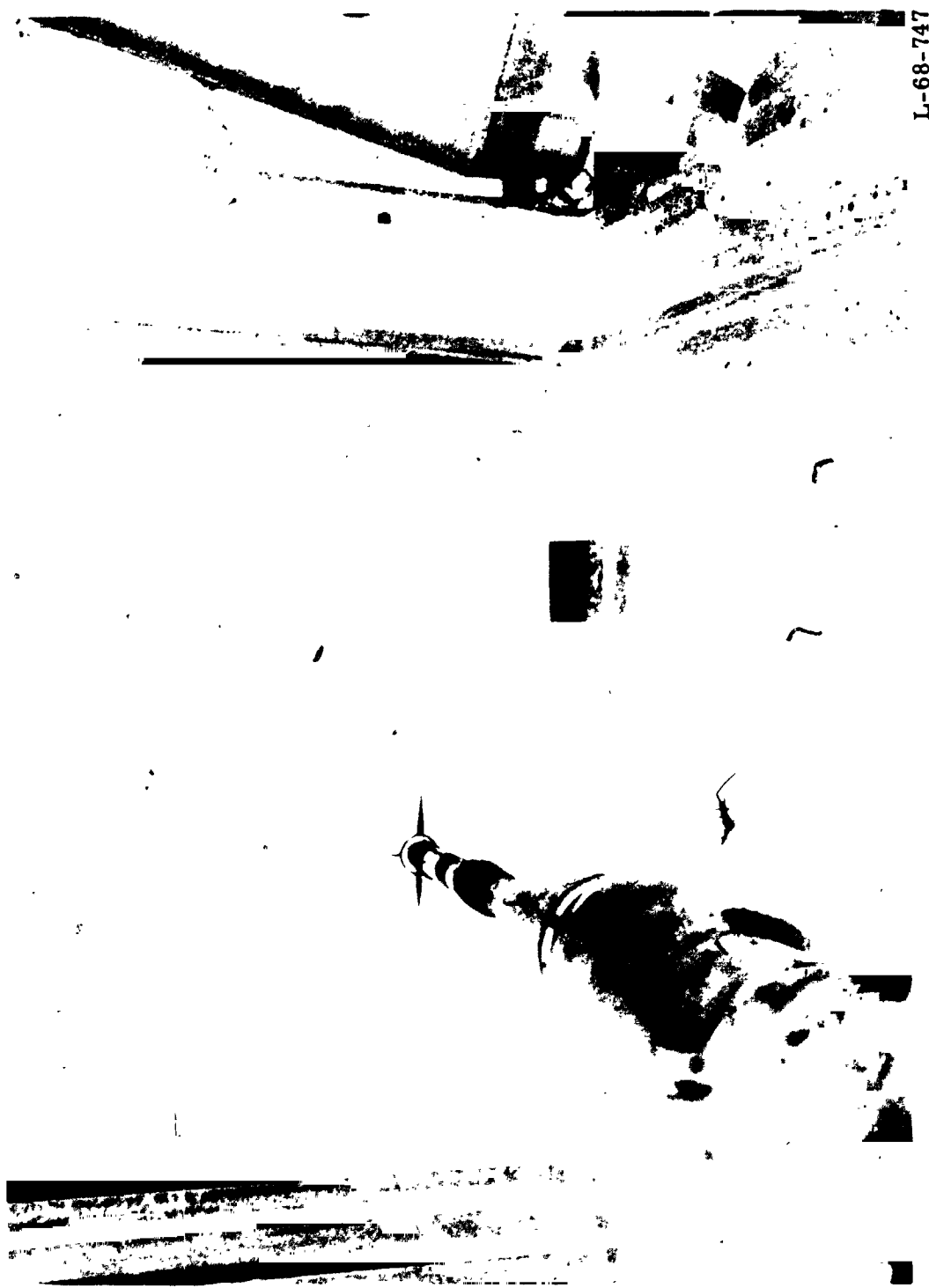
Figure 1.- Concluded.



L-67-6378

(a) Subsonic model (without vertical tail) installed in Langley 7- by 10-foot high-speed tunnel.

Figure 2.- Typical photographs of models installed in wind tunnels.



L-68-747

(b) Supersonic model installed in Langley Unitary Plan wind tunnel.

Figure 2.- Continued.



L-70-8749

(c) Hypersonic model in Langley continuous-flow hypersonic tunnel.

Figure 2.- Concluded.

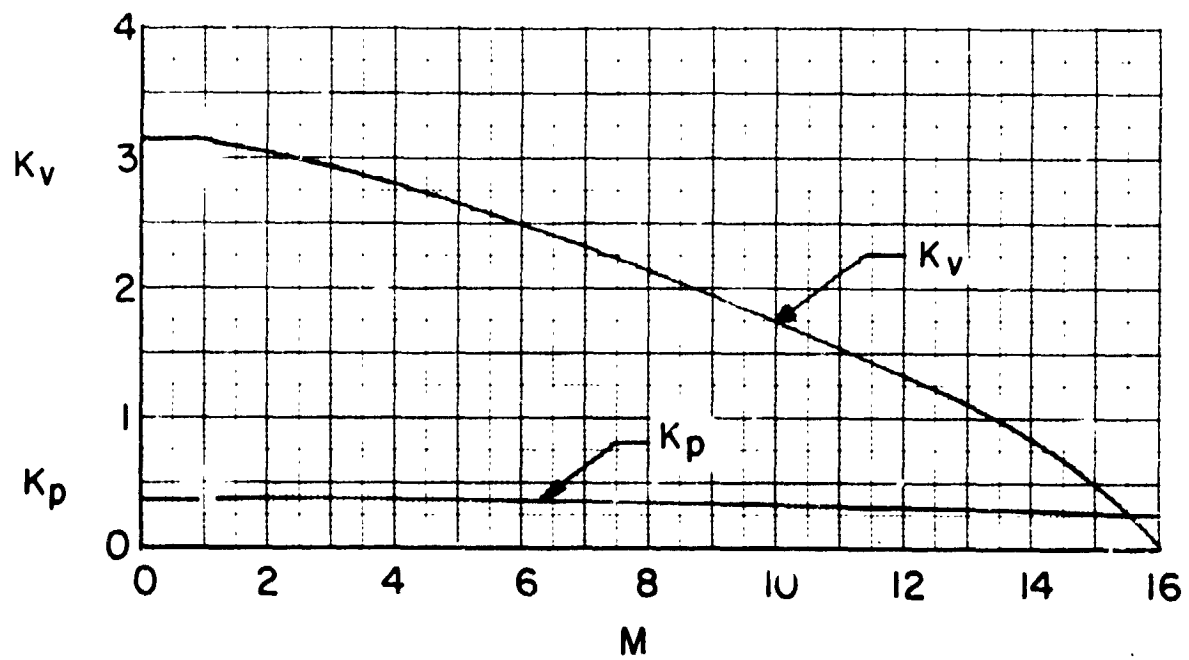
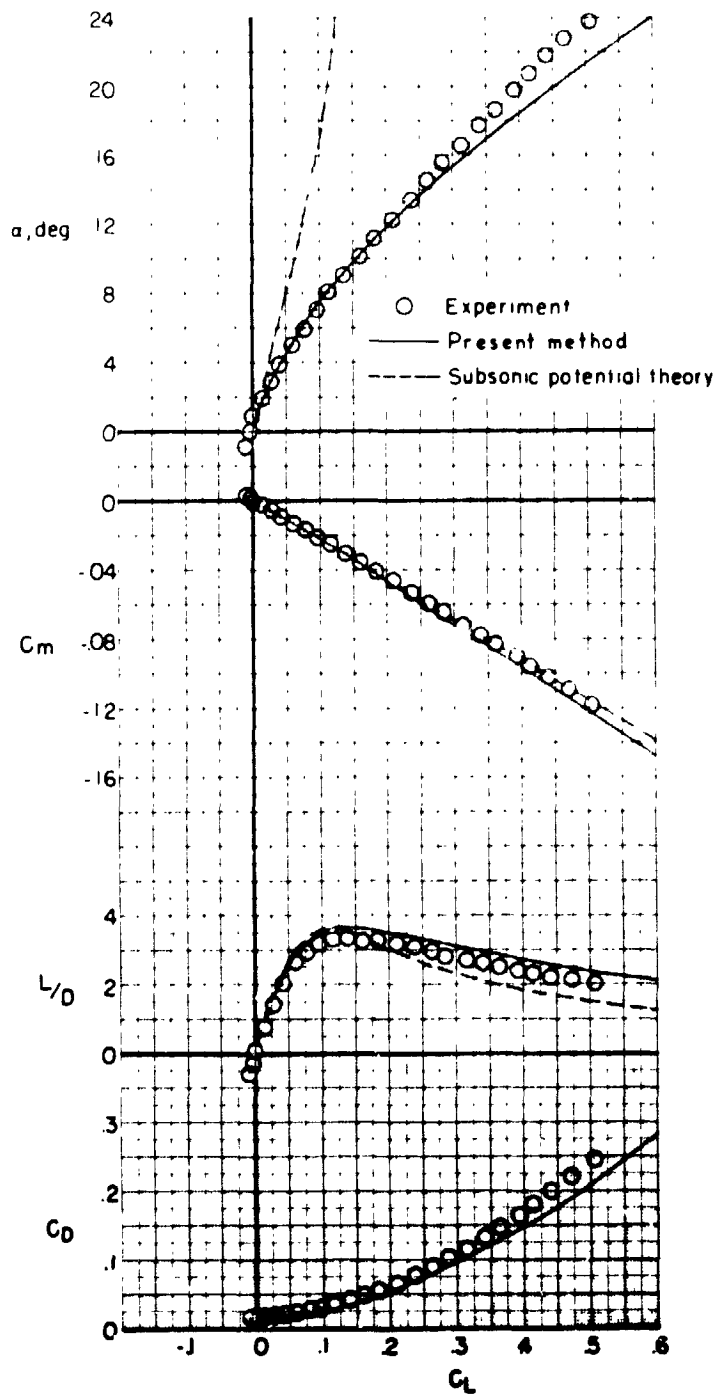
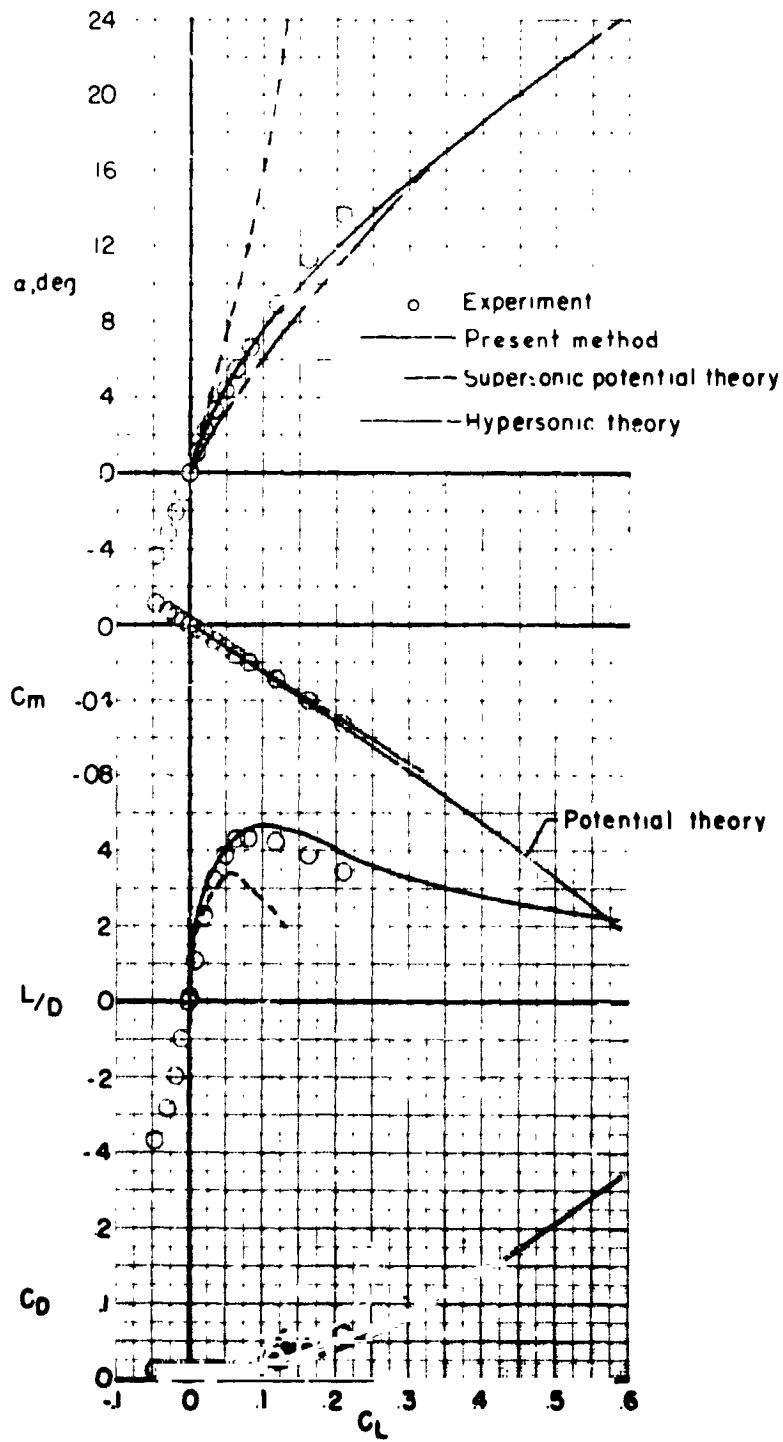


Figure 3.- Variation of K_p and K_v with Mach number for aspect ratio 0.25 wing where K_v is based on leading-edge suction analogy.



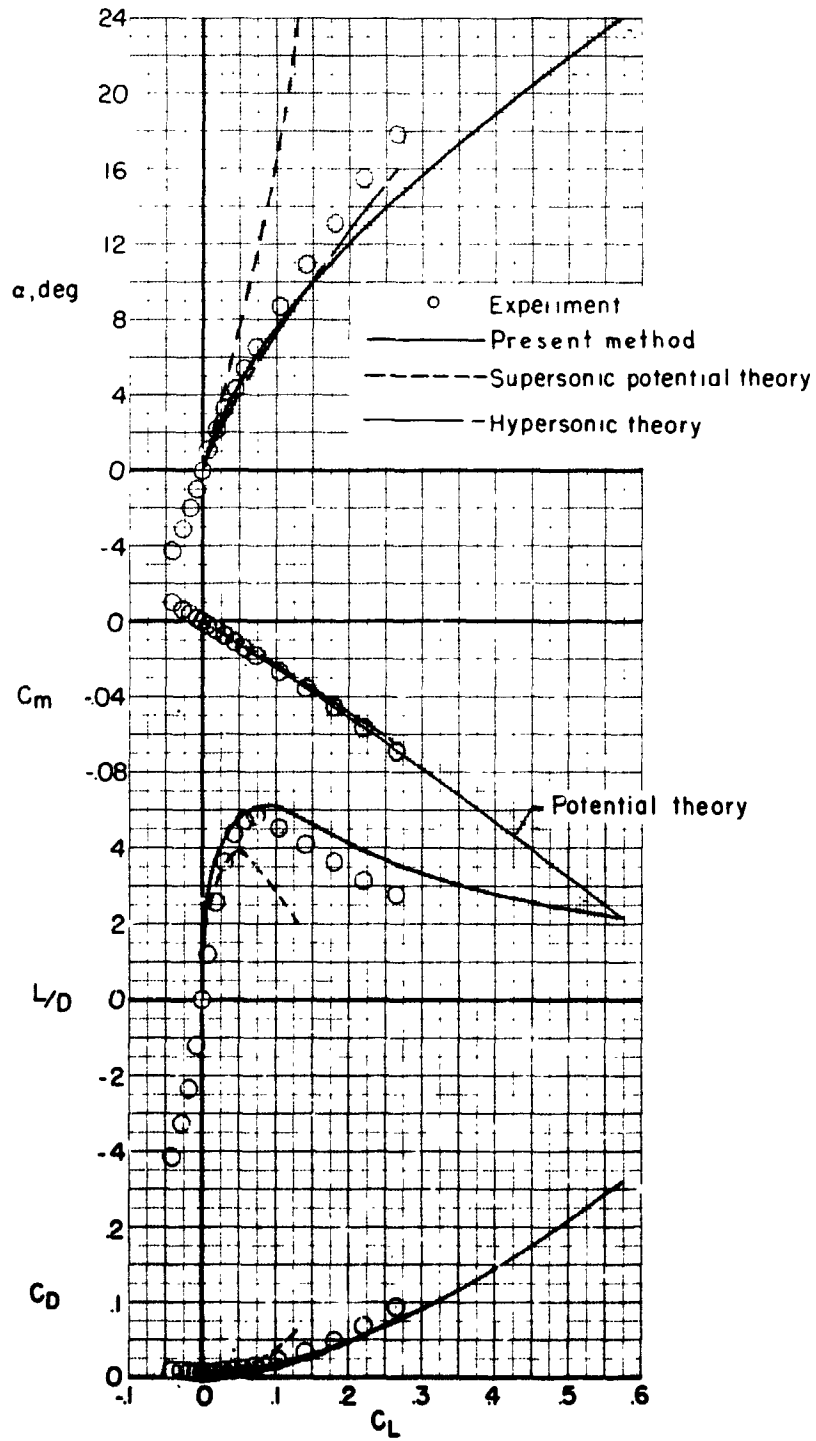
(a) $M = 0.143$.

Figure 4.- Experimental results and theoretical predictions for some longitudinal aerodynamic characteristics of aspect ratio 0.25 wing.



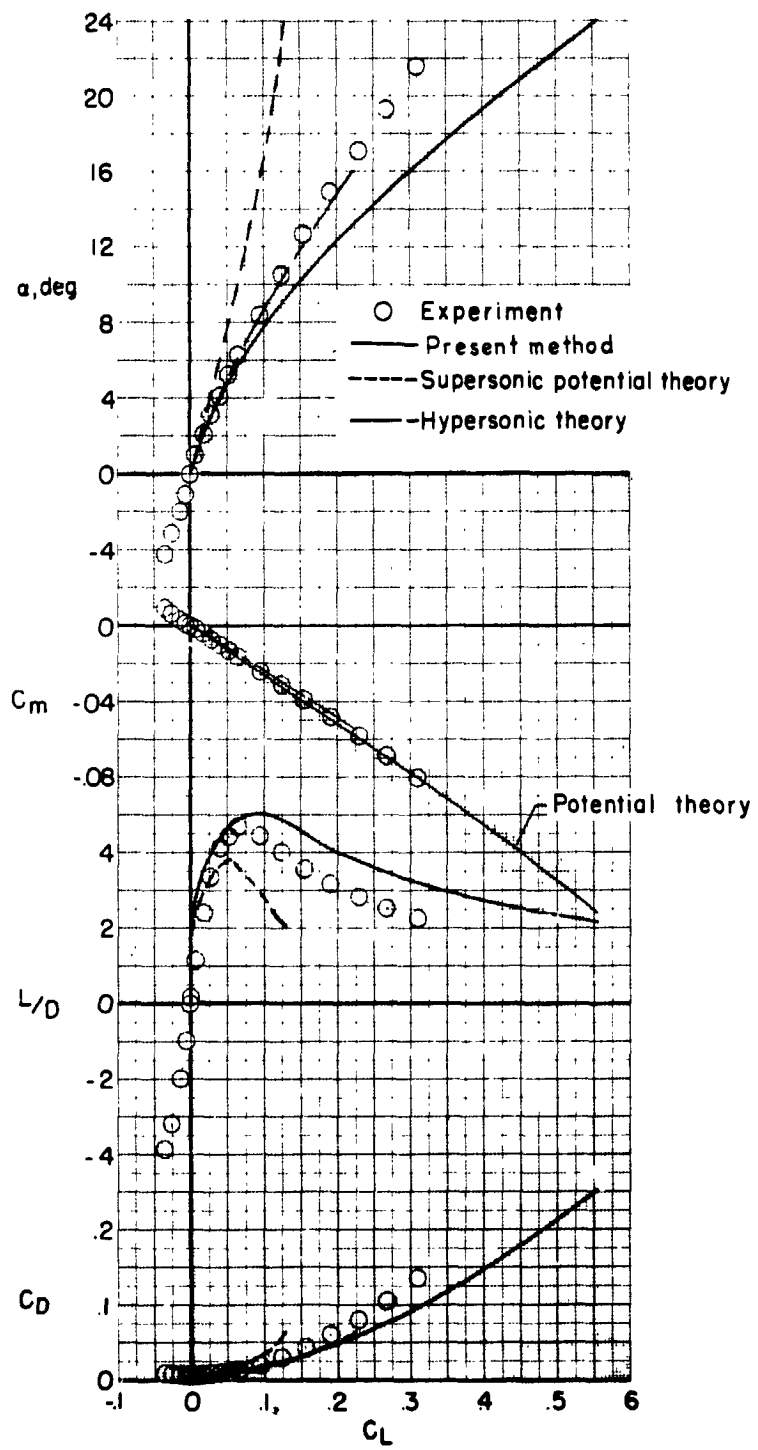
(b) $M = 2.30$.

Figure 4.- Continued.



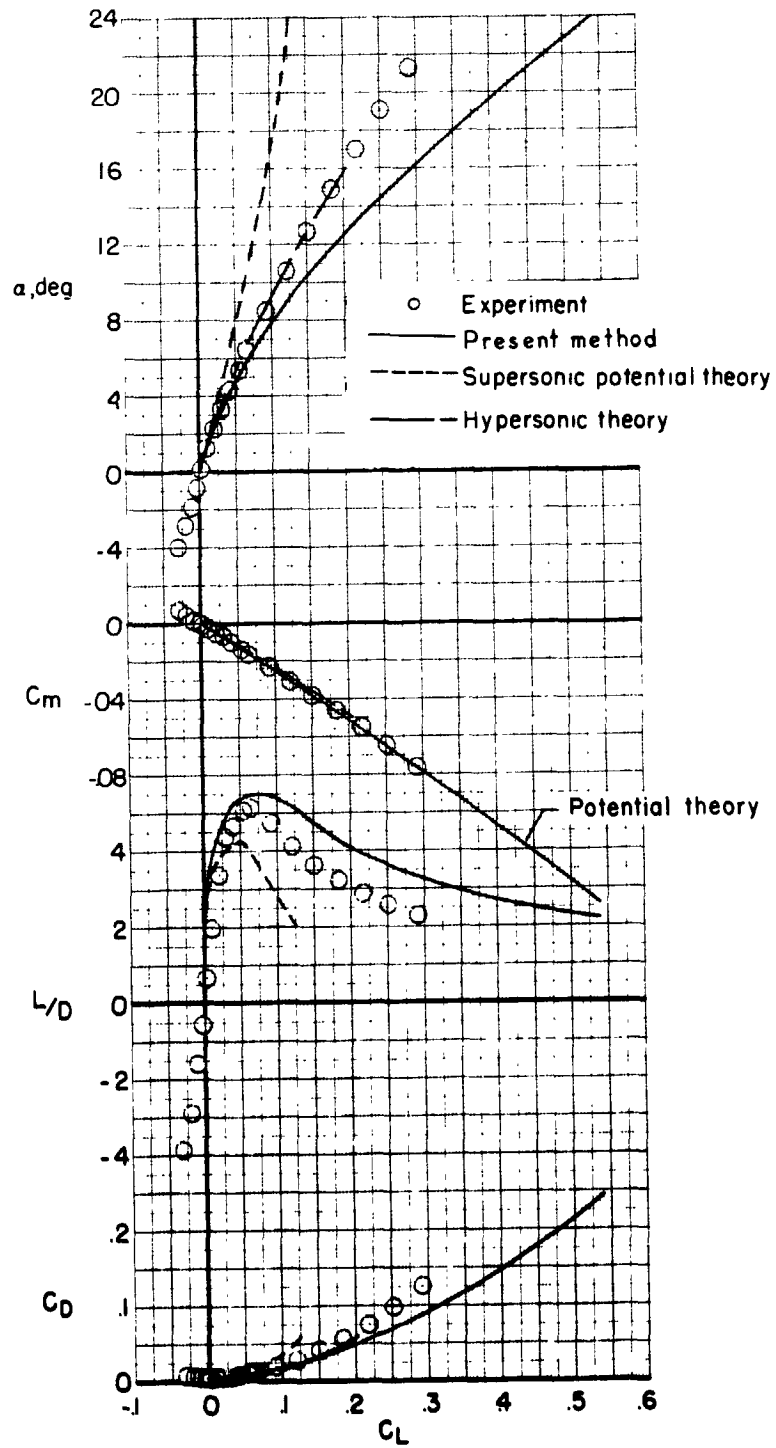
(c) $M = 2.96$.

Figure 4.- Continued.



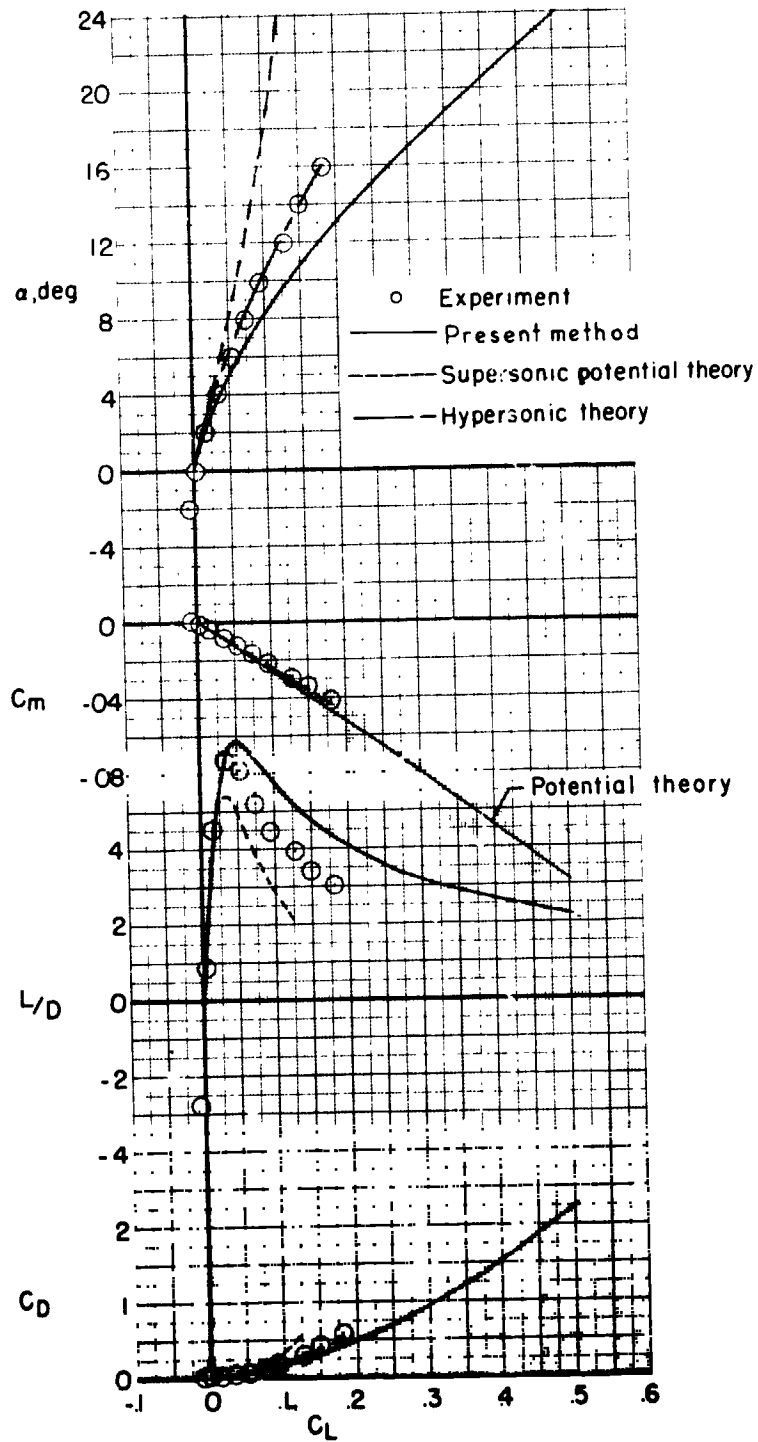
(d) $M = 3.95$.

Figure 4.- Continued.



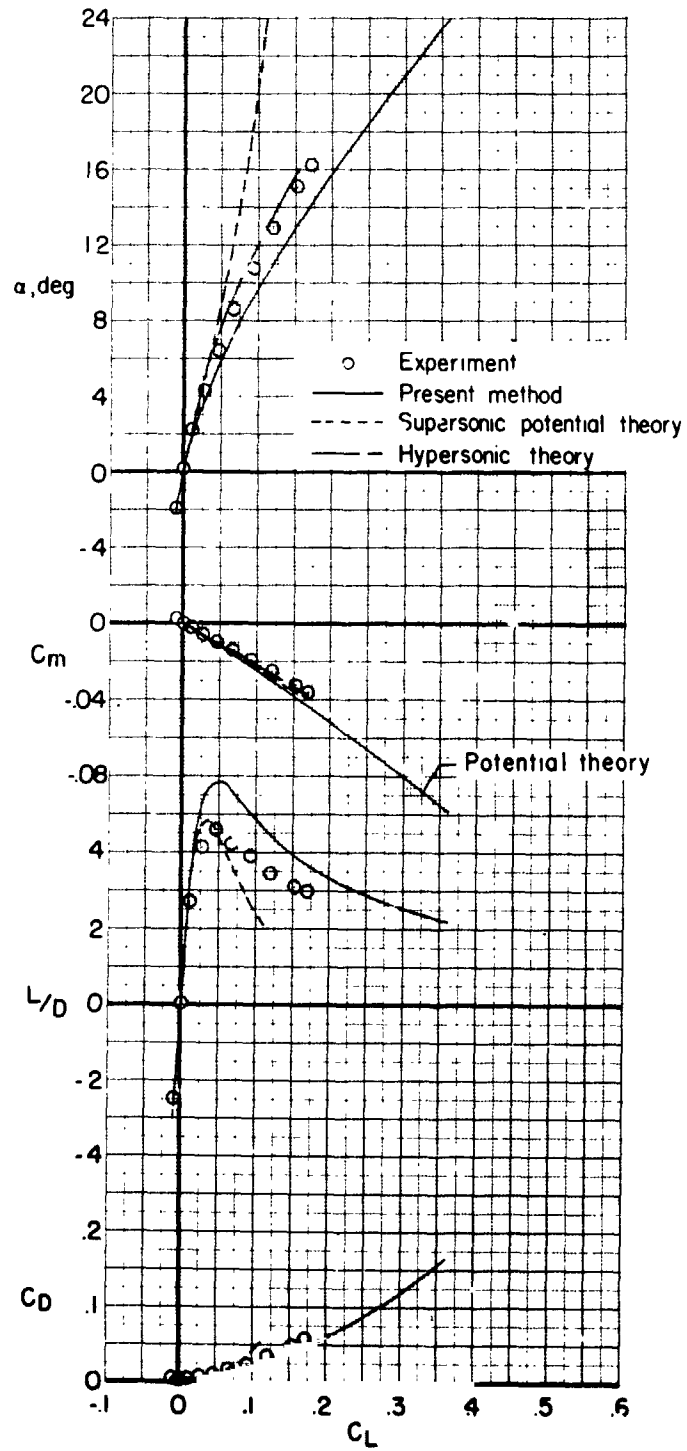
(e) $M = 4.63$.

Figure 4.- Continued.



(f) $M = 5.99$.

Figure 4.- Continued.



(g) $M = 10.40$.

Figure 4.- Concluded.

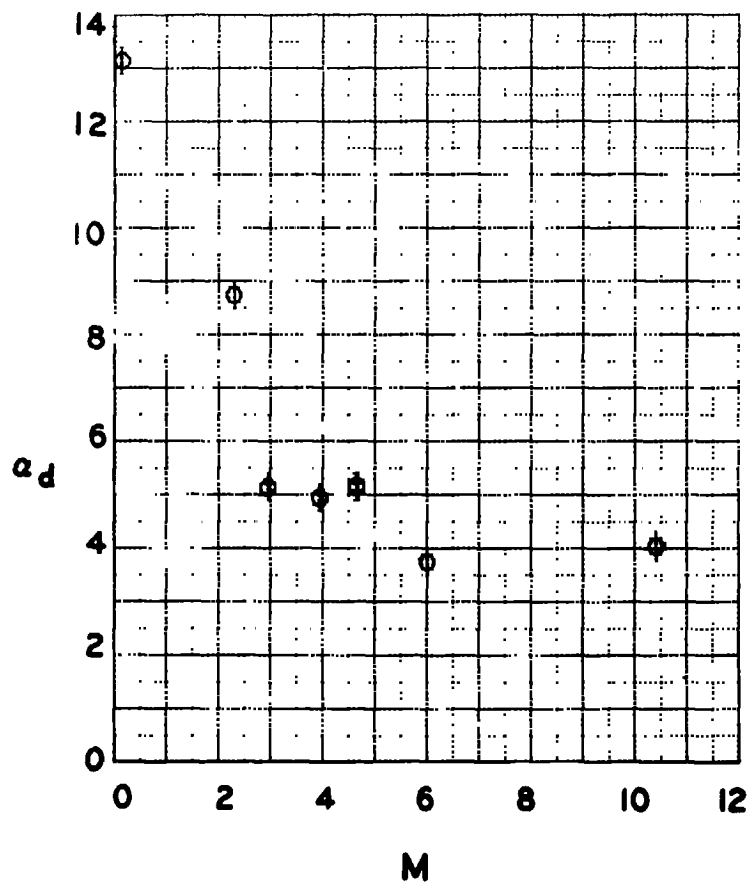


Figure 5.- Effect of Mach number on angle of attack at which present method predictions and experimental values for C_{L_c} begin to depart.

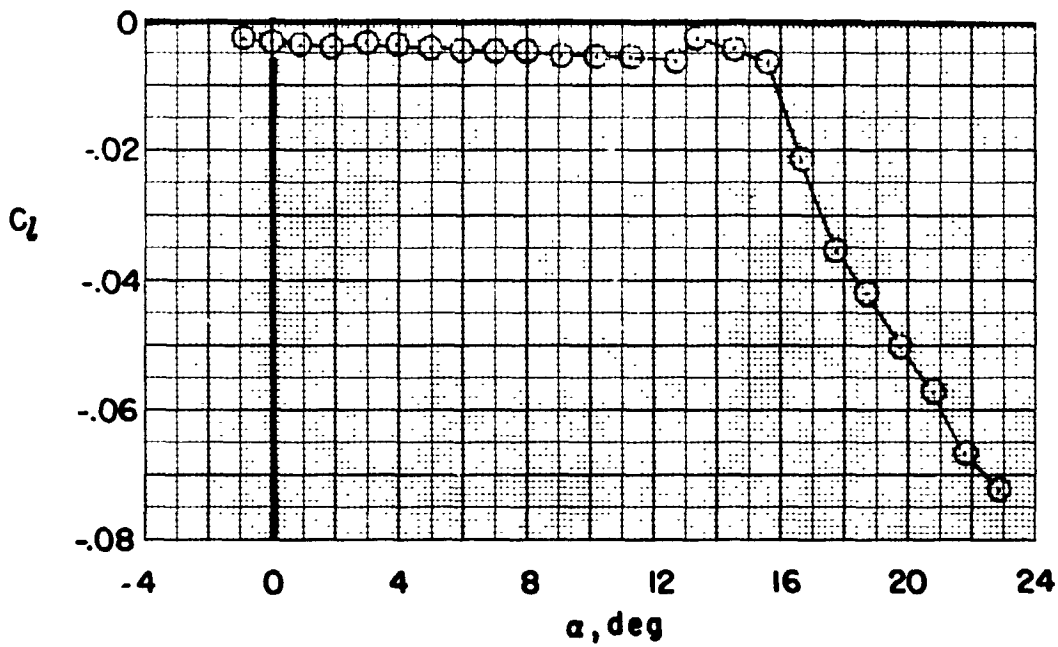
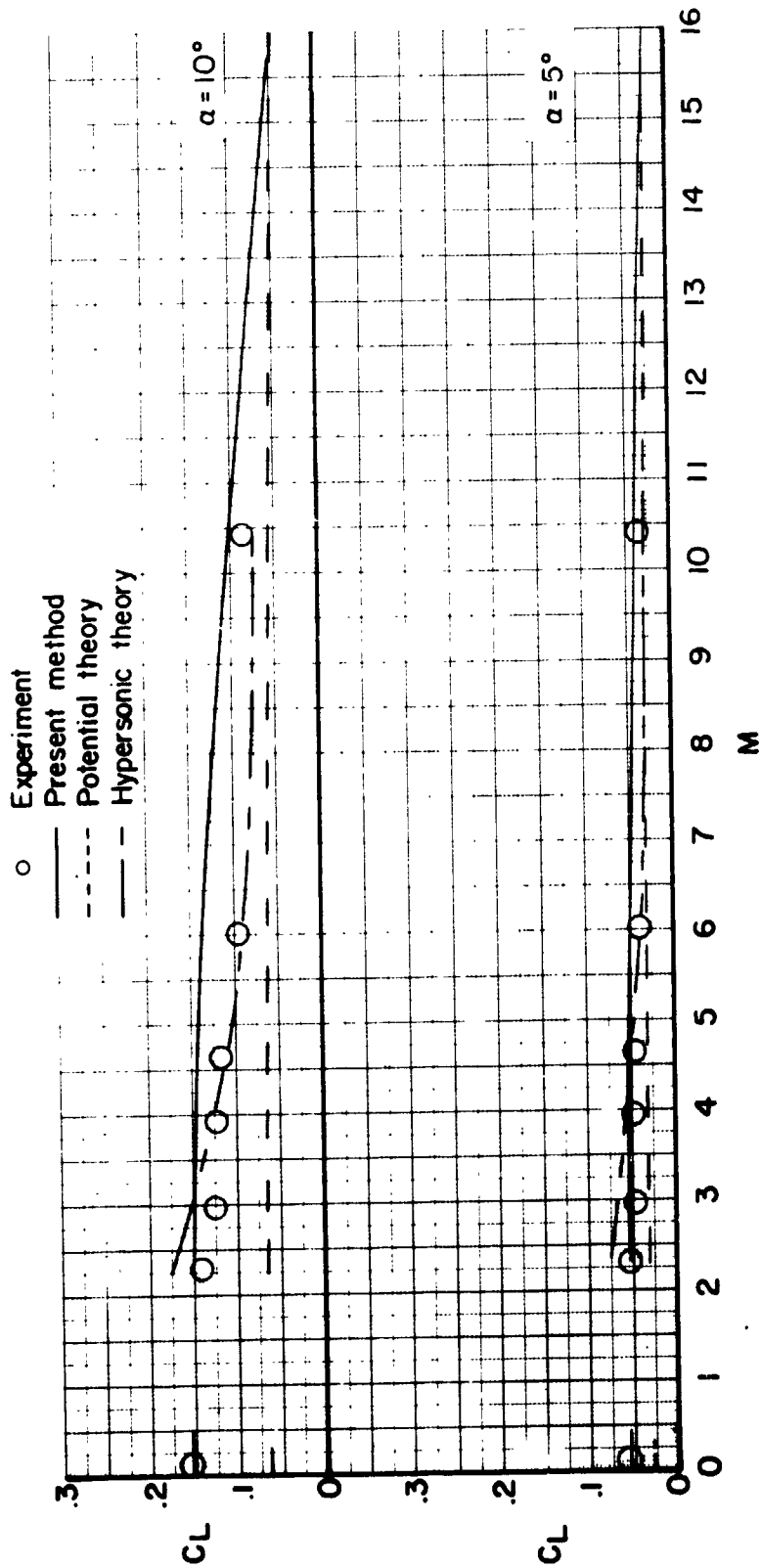
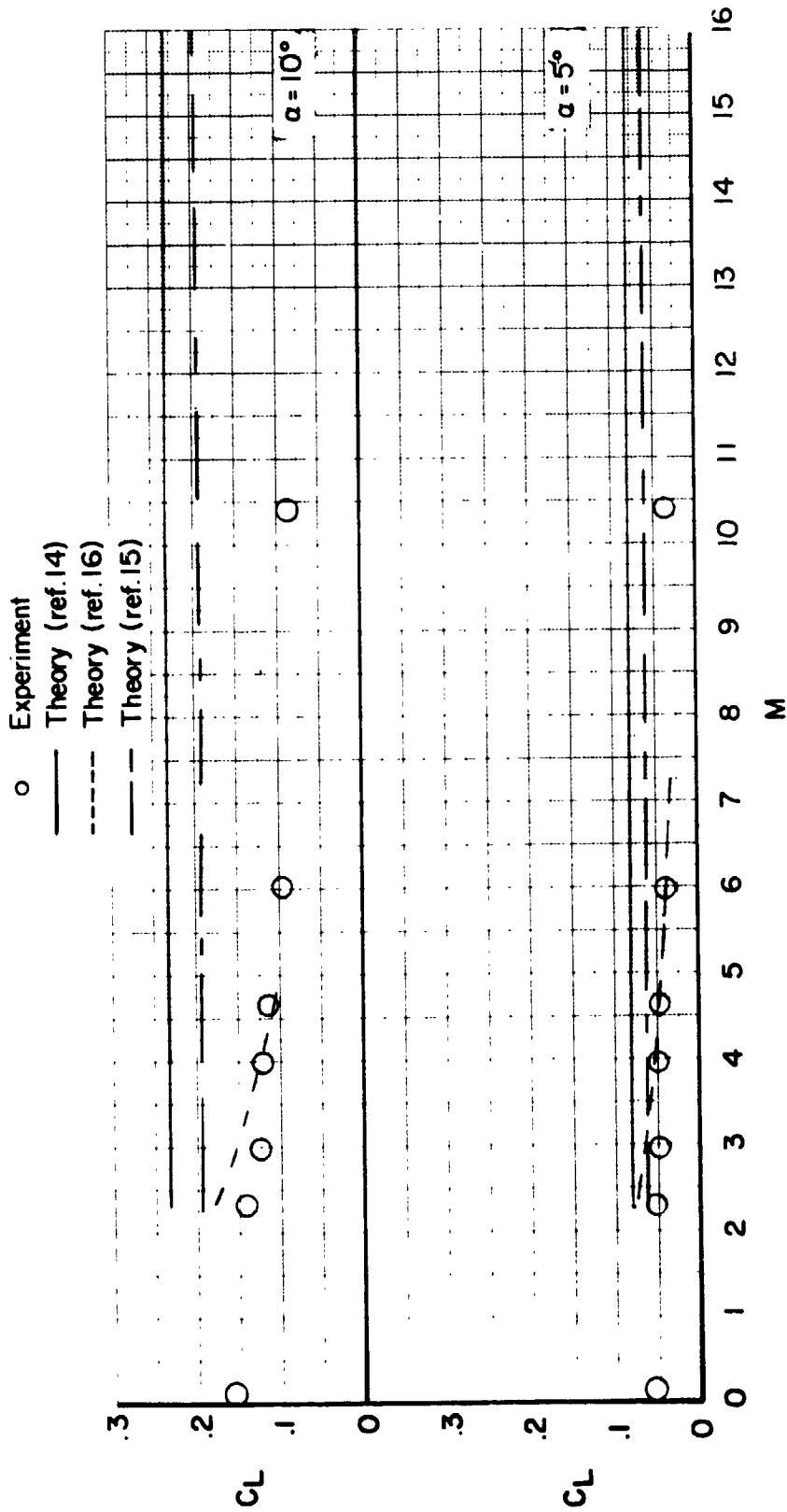


Figure 6.- Variation of rolling-moment coefficient with angle of attack for aspect ratio 0.25 wing at $M = 0.143$.

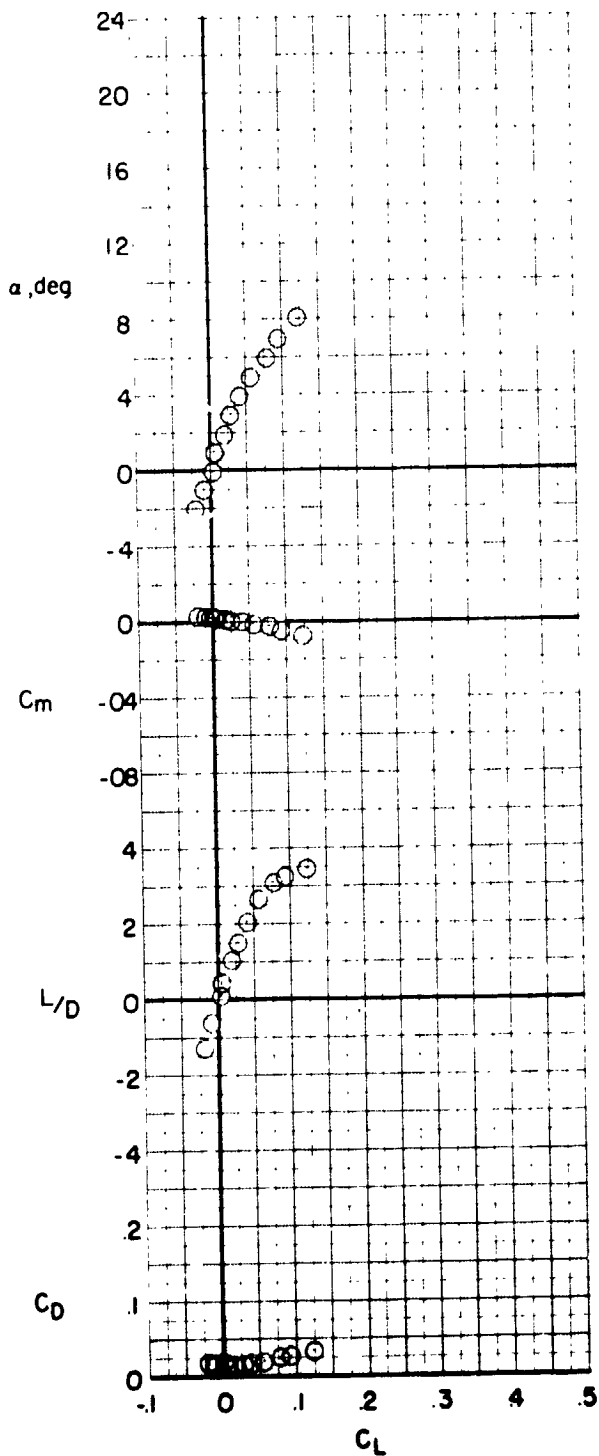


(a) Comparison with theories of this paper.
 Figure 7.- Variation of selected theoretical and experimental lift coefficients for aspect ratio 0.25 wing as function of Mach number.

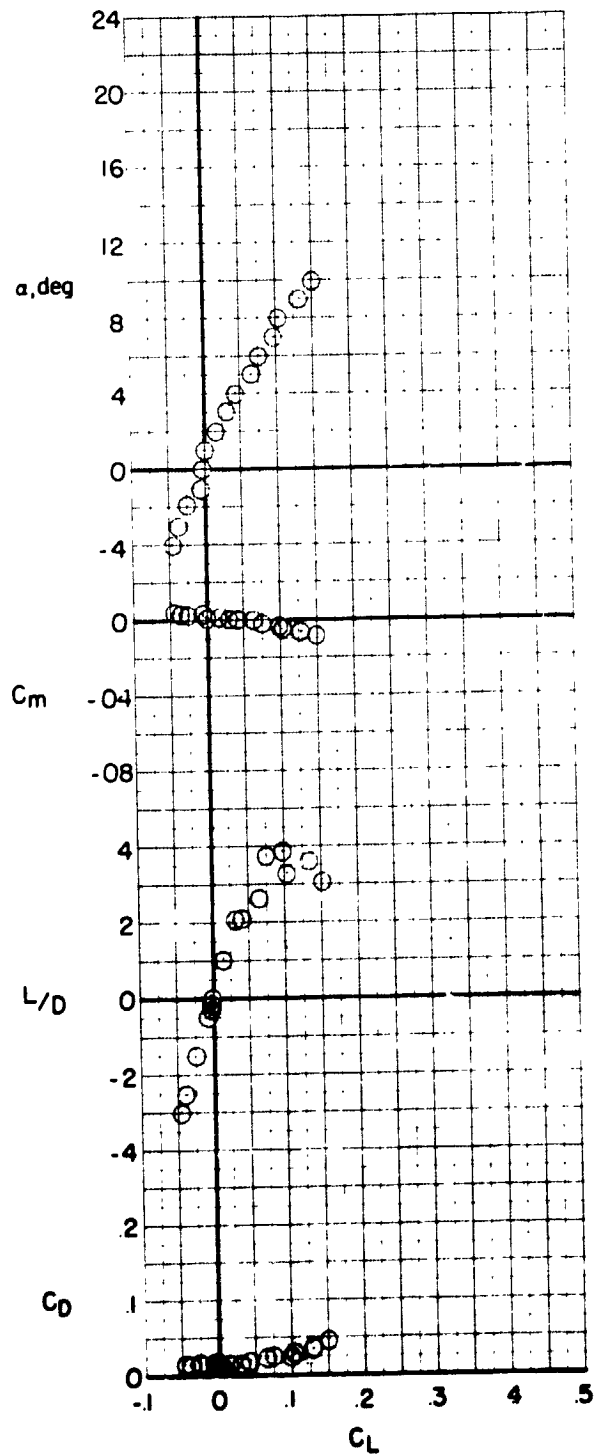


(b) Comparison with other theories which account for effect of leading-edge vortex.

Figure 7.- Concluded.

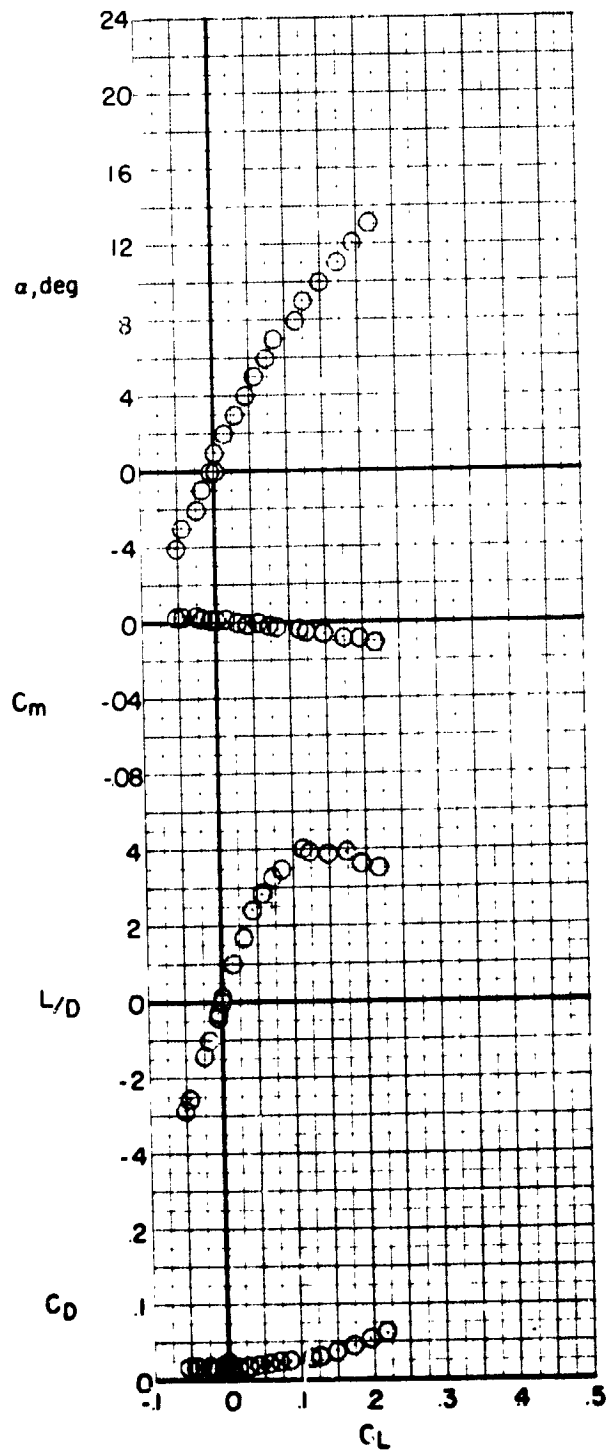


(a) $\frac{h\bar{c}}{4} = 0.166.$

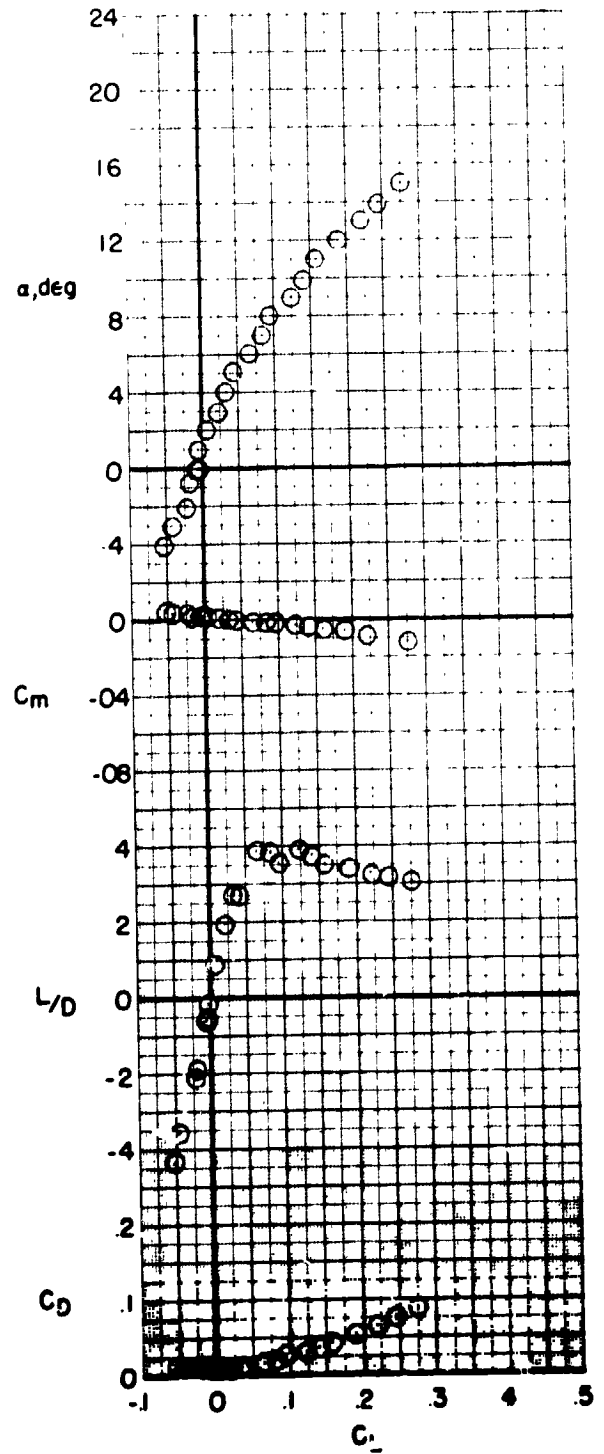


(b) $\frac{h\bar{c}}{4} = 0.20.$

Figure 8.- Experimental longitudinal aerodynamic characteristics of aspect ratio 0.25 wing at $M = 0.074$ in ground proximity.

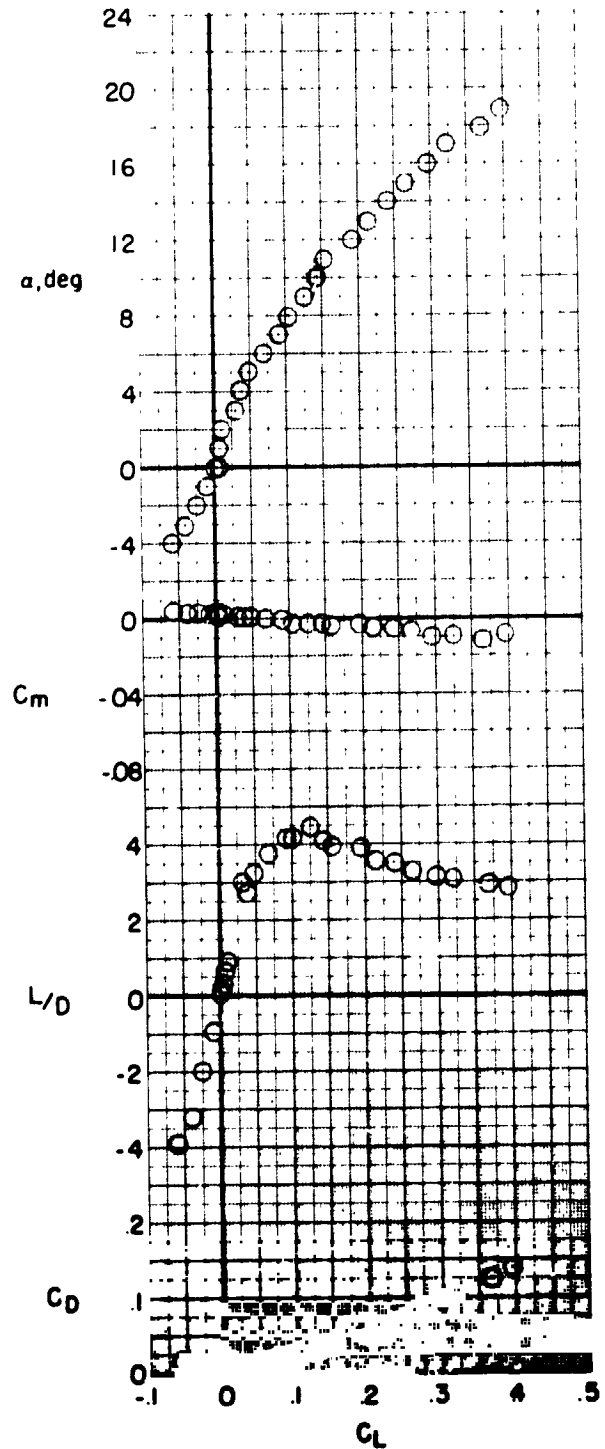


(c) $\frac{h_c/4}{c} = 0.25.$

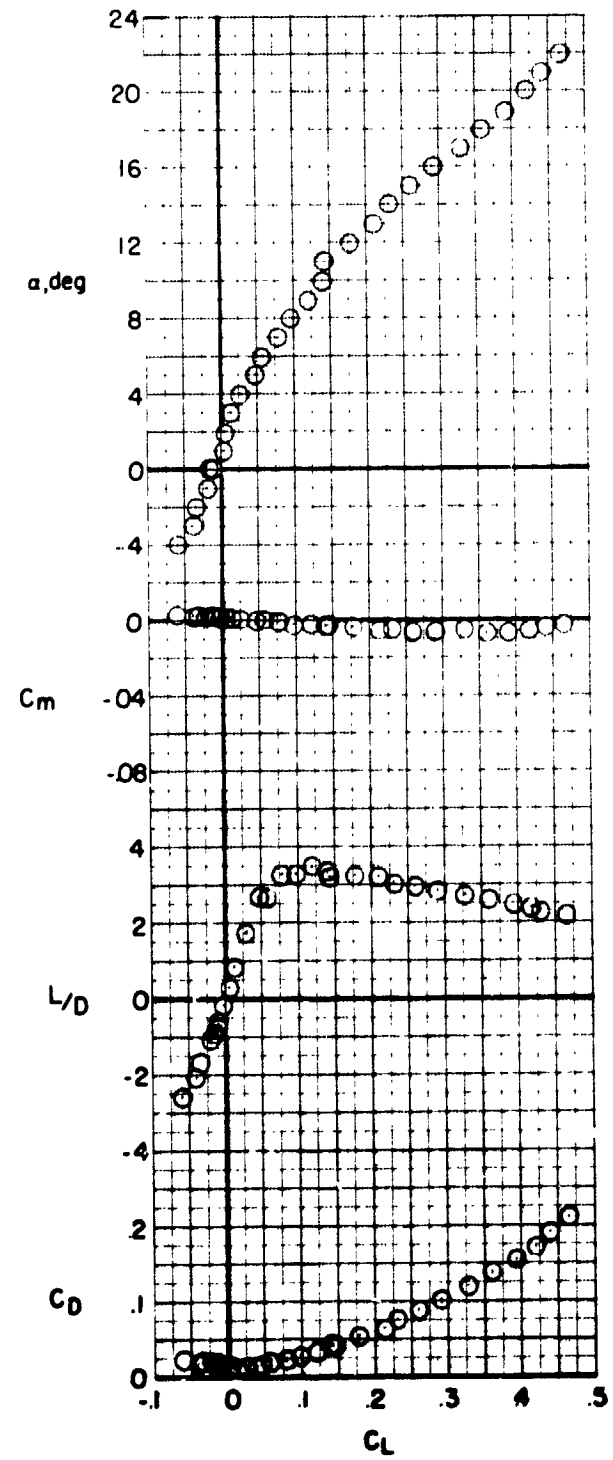


(d) $\frac{h_c/4}{c} = 0.292.$

Figure 8.- Continued.

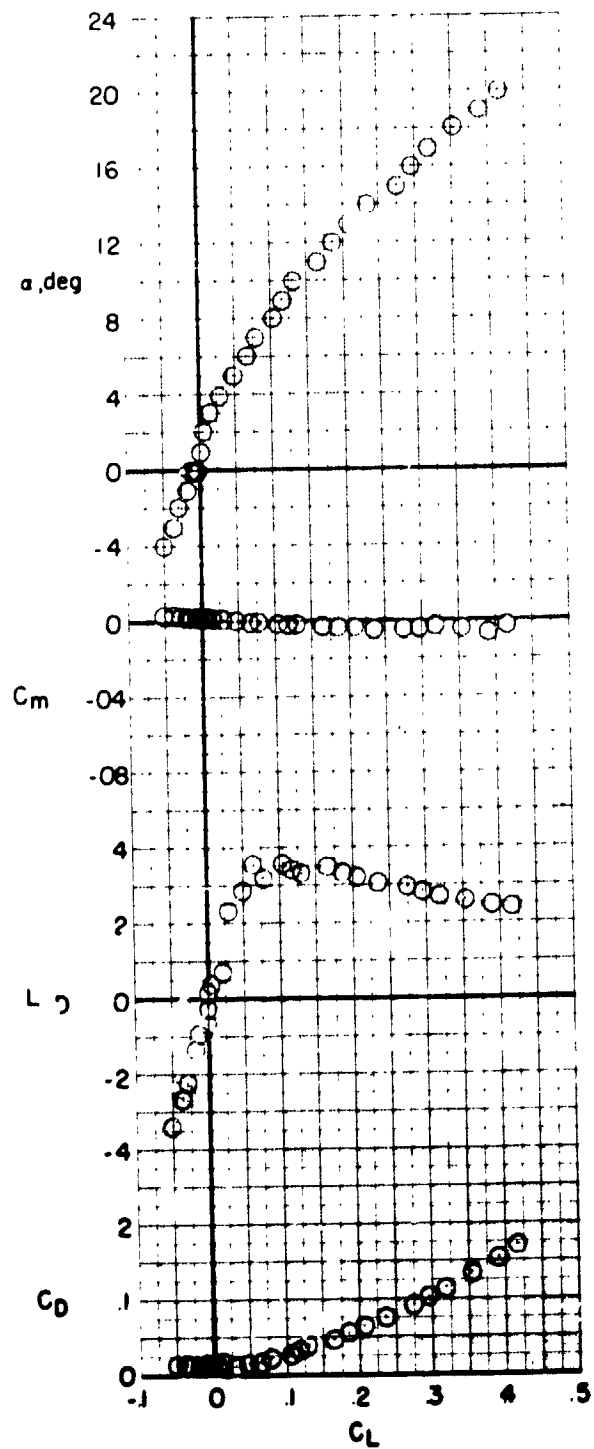


(e) $\frac{h_c/4}{c} = 0.35.$

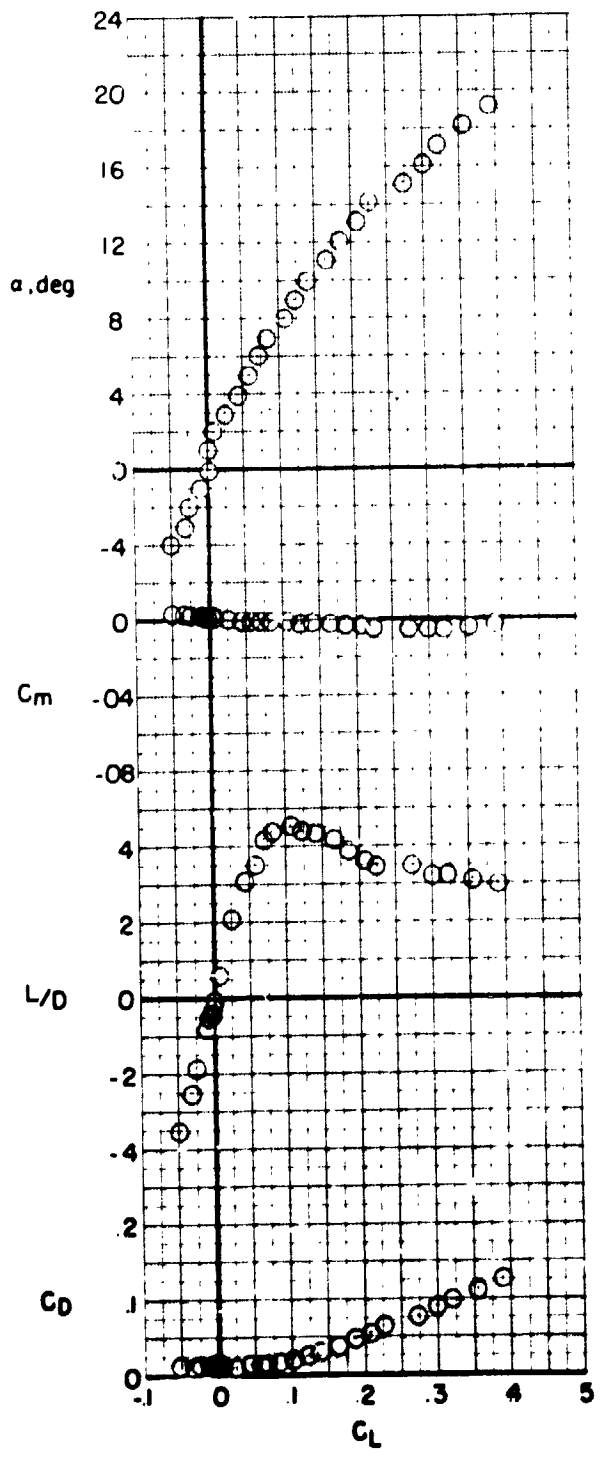


(f) $\frac{h_c/4}{c} = 0.45.$

Figure 8.- Continued.

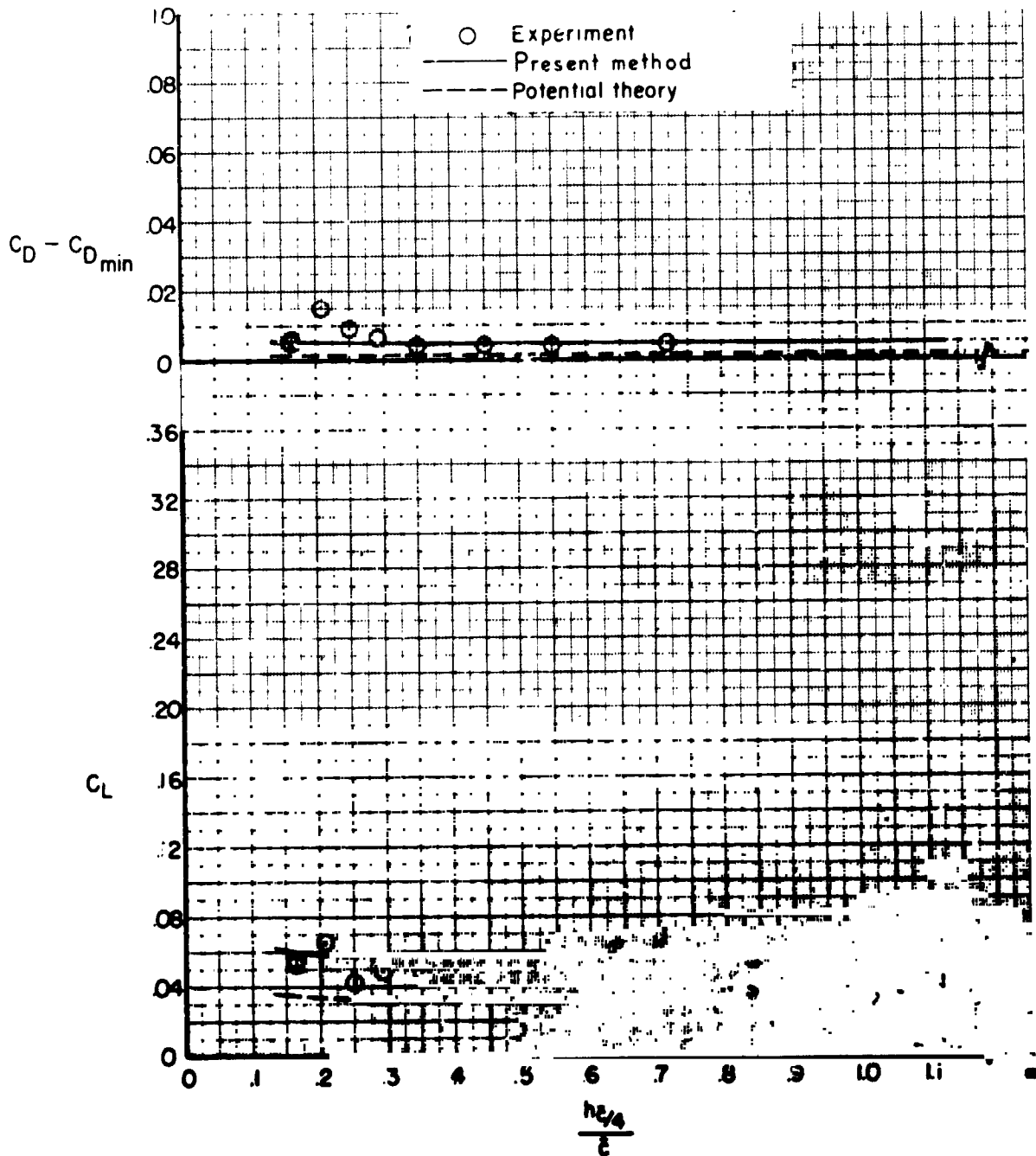


(g) $\frac{h_c}{4} = 0.55.$



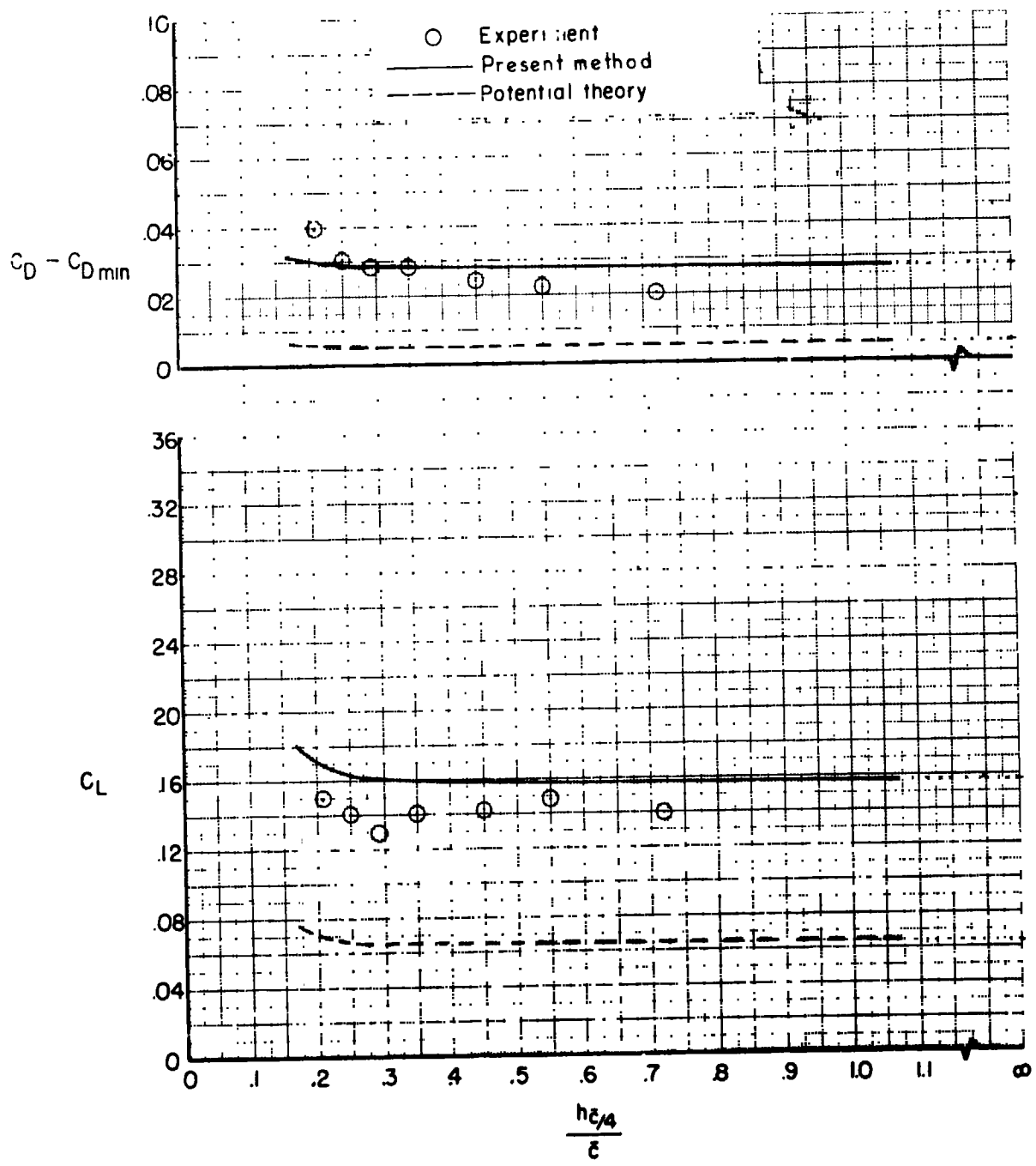
(h) $\frac{h_c}{4} = 0.72.$

Figure 8.- Concluded.



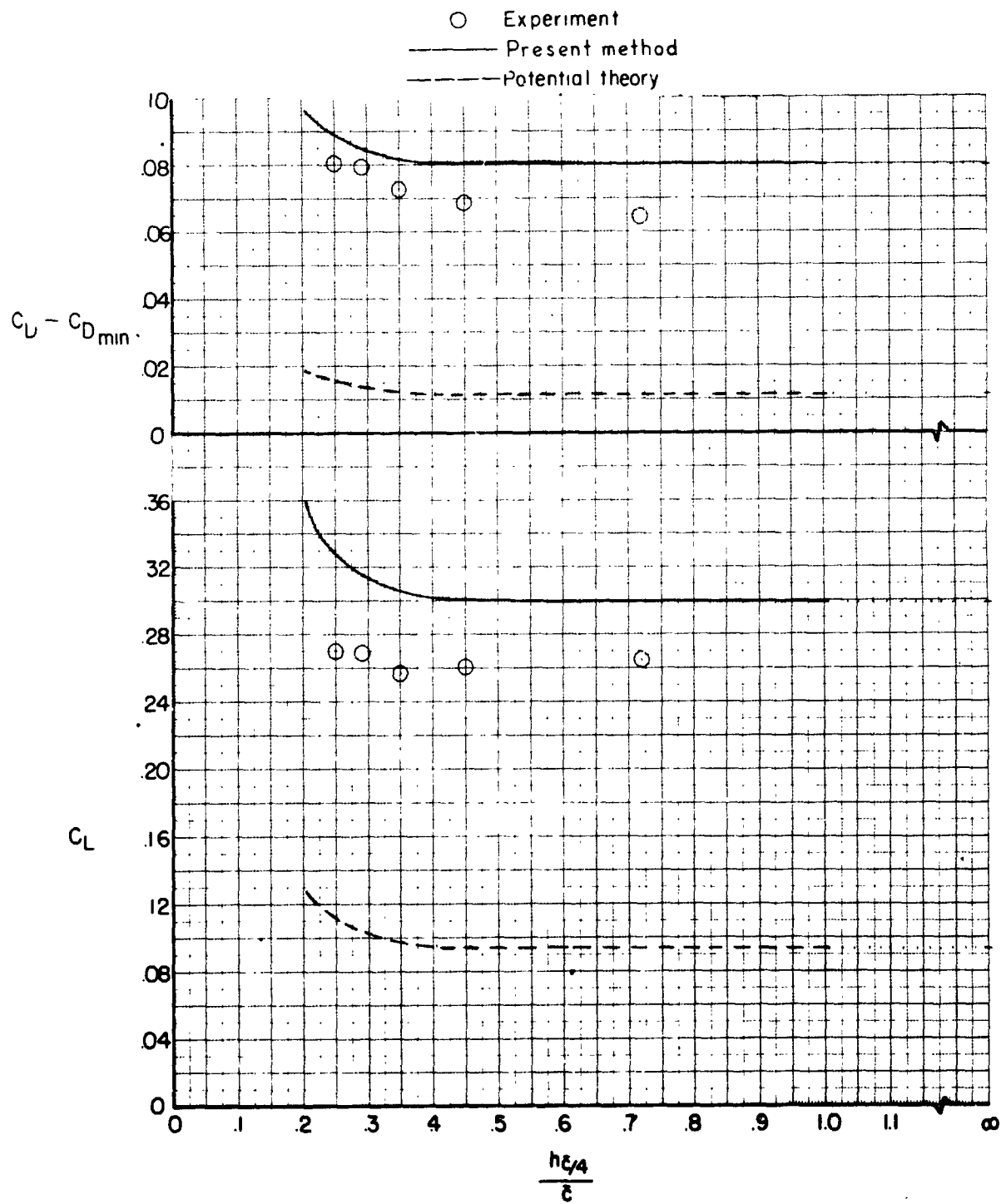
(a) $\alpha = 5^\circ$.

Figure 9.- Experimental results and theoretical predictions for some longitudinal aerodynamic characteristics of aspect ratio 0.25 wing at $M = 0.074$ in ground proximity.



(b) $\alpha = 10^\circ$.

Figure 9.- Continued.



(c) $\alpha = 15^\circ$.

Figure 9.- Concluded.

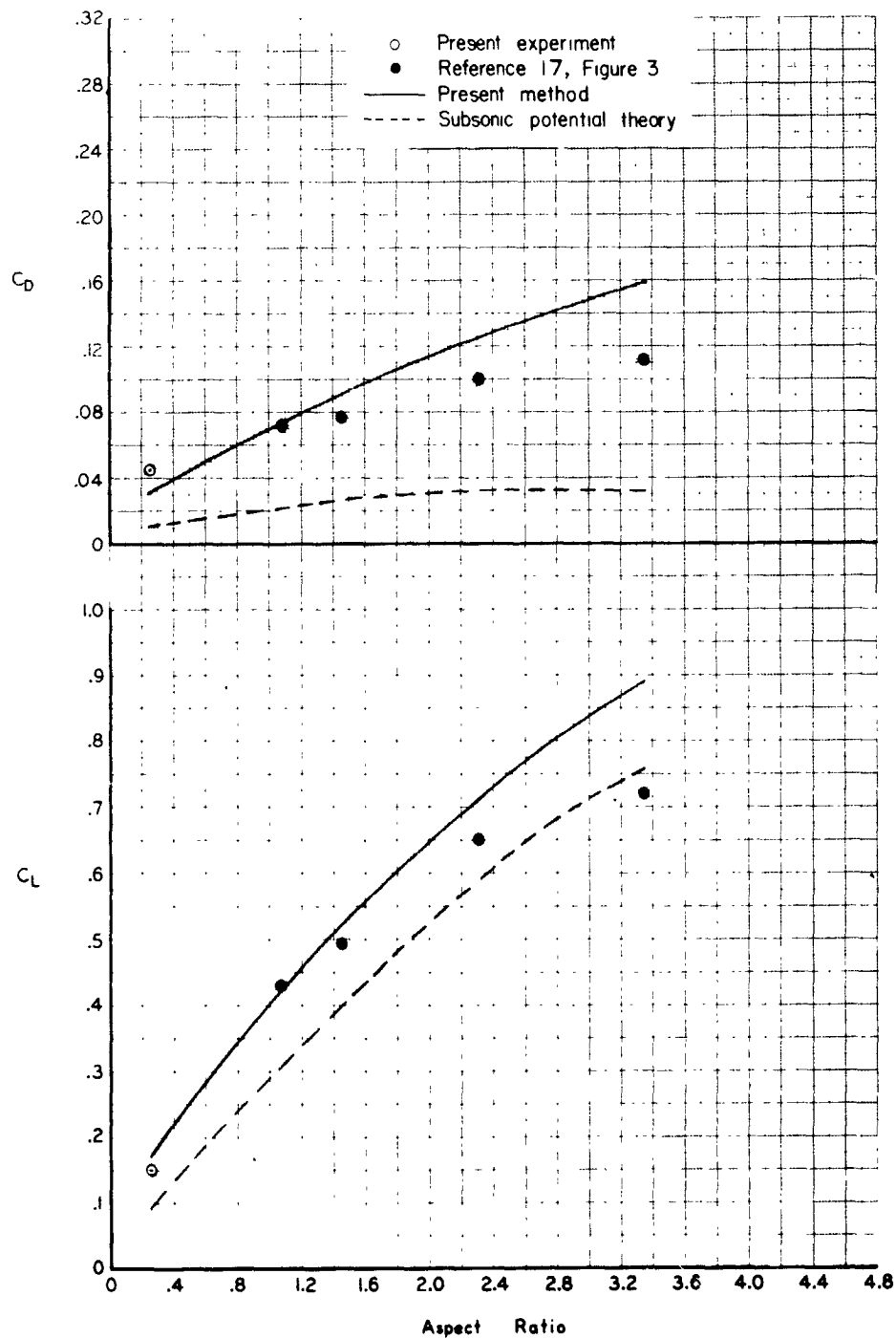


Figure 10.- Summary of lift and drag comparisons of theory and experiment in ground proximity at angle of attack of 10° (Note that data and theory at aspect ratio 0.25 are at $\frac{h\bar{c}/4}{\bar{c}} = 0.20$, whereas data of ref. 17 are at $\frac{h\bar{c}/4}{\bar{c}} = 0.238$.)

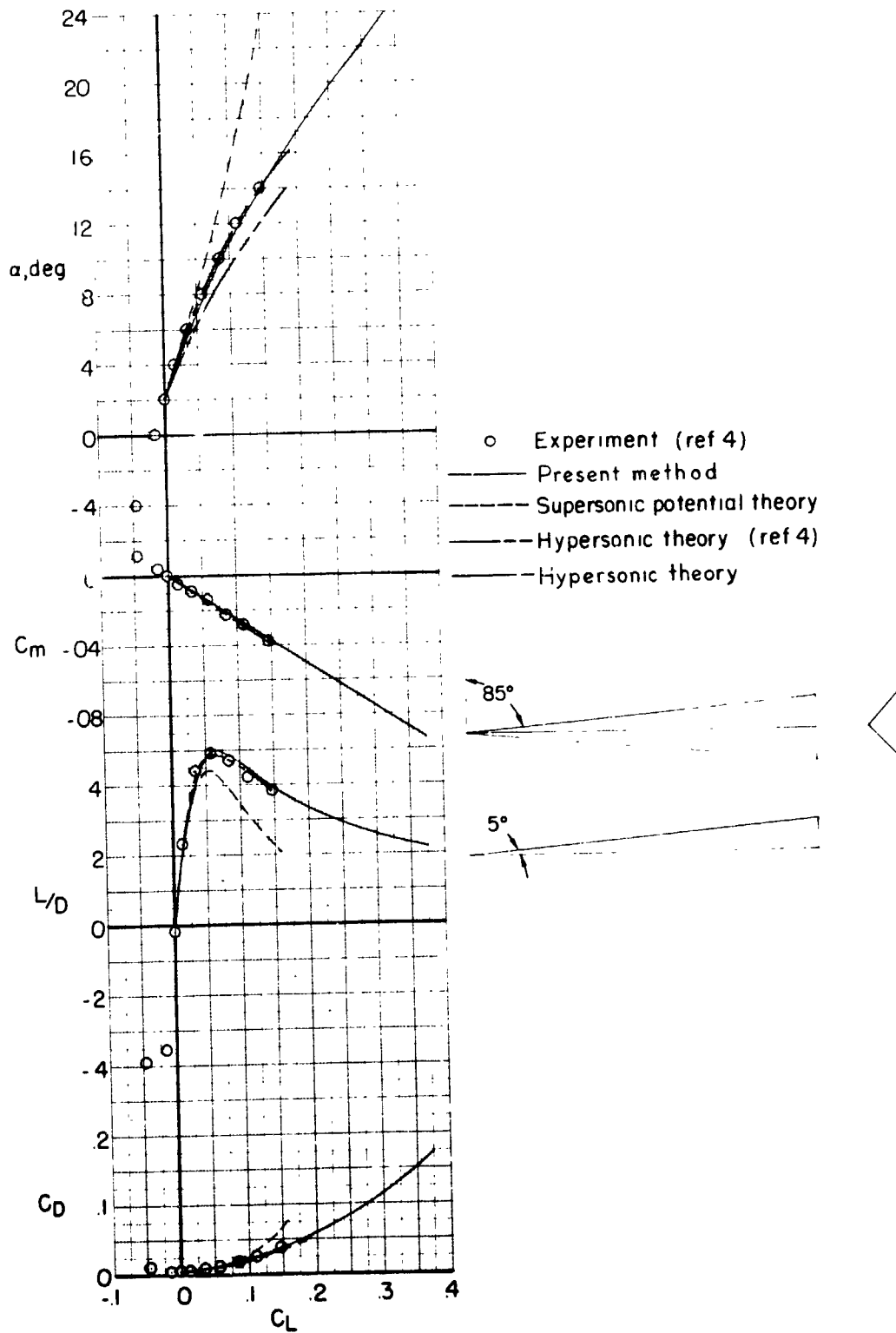


Figure 11.- Experimental results and theoretical predictions for some longitudinal aerodynamic characteristics of aspect ratio 0.35 triangular cross-sectional body at $M = 6.9$.